

Response to “Changing pattern of ice flow and mass balance for glaciers discharging into the Larsen A and B embayments, Antarctic Peninsula, 2011 to 2016”

The Cryosphere Discuss., <https://doi.org/10.5194/tc-2017-259>

Authors: Rott, H., Abdel Jaber, W., Wuite, J., Scheiblaue, S., Floricioiu, D., van Wessem, J.M., Nagler, T., Miranda, N., van den Broeke, M.R.

Line numbers in the response refer to the revised version with changes tracked, dated 2018-03-07

In the revised manuscript the figure numbers are shifted by 1 because an additional figure (new Figure 1) was added. This figure, demonstrating excellent agreement between elevation change measured by IceBridge airborne lidar and TanDEM-X, responds to a critical question of Interactive Comment SC1 regarding the quality of the TanDEM-X DEM differencing analysis.

Referee comments in italic

Anonymous Referee #1

Comment: *The paper presents the results of a new analysis of elevation change and flow speed change for the eastern Antarctic Peninsula from Sjogren-Boydell glacier to Leppard Glacier, spanning the major outlets on the mainland Peninsula that were affected by the loss of ice shelves in 1995 and 2002. The study shows that the systems have moved in a positive direct in mass balance (either less negative, or positive outright) in the past few years. They attribute the decline of loss rate to the persistent presence of fast ice in the embayments.*

This is a very clear and well-written study, with a lot of good (accurate) new data to offer. It could be published as it is. It provides a ‘next chapter’ in the monitoring of this rapidly-changing region impacted by ~25 years of very warm conditions (1980-2006) which have tapered to slightly cooling over the past several years (still warmer than the mid-20th century by a considerable amount). Even at this point, two decades past the ice shelf disintegrations, the glacier systems still show short-term changes in both elevation and flow speed.

Attribution of the reduction in ice losses (less negative mass balance, and in some cases a switch to positive mass balance) is given to a reduction in calving flux – i.e. a downstream movement of the calving front. This in turn is attributed to persistent fast ice.

Minor comments follow.

Response: We are glad about the very positive feedback on the scope of our work and would like to thank the reviewer for the helpful comments, providing very valuable support for improving the quality of the manuscript. We carefully took into account these comments for revising the manuscript, as explained in the detailed response below.

Comment: *I would encourage the authors to adopt a consistent sign convention for mass budget / mass balance, i.e. negative means ice mass leaving the system. Although there is not*

a great deal of ambiguity (the words and numbers match the meaning everywhere I have checked), in places one wonders if a positive 'loss' might mean a net gain or a net loss, etc.

Response: We now use consistently mass balance (negative for losses, positive for gain).

Changes in manuscript: This sign convention is now used throughout the manuscript.

Comment: L22 please use 'mass budget method' rather than 'input-output' method. Note that IMBIE-2 has now adopted this phrasing.

Changes in manuscript: Everywhere changed as proposed.

Comment: L32 no need to preface the mass budget results with ' $B_n =$ ' – it's a bit confusing, since you have not introduced that variable name, and not necessary.

Changes in manuscript: Changed. B_n deleted in the Abstract.

Comment: L32 Also – L34 a 'mass loss' for a glacier losing mass would be –positive- : these are mass balance results, so negative numbers already mean 'loss'. A picky point, but this has been made strenuously by other authors/speakers.

Changes in manuscript: Changed. Mass balance numbers are now used throughout the abstract.

Comment: L41 this 'sea ice cover' was/is 'landfast ice' – another picky point perhaps, but an upcoming paper will discuss this buttressing, and fast ice is a much better buttress than typical sea ice.

Response: The proglacial fjords were actually filled by ice mélange extending several kilometres in front of the glaciers and by sea ice of different age farer away and also in the main sections of the Larsen A and B embayments.

Changes in manuscript: In L42, L43 (revised manuscript) we change the wording to "when ice mélange and sea ice cover persisted in the proglacial fjords and bays during summer." We address the topic of ice mélange in the revised discussion section.

Comment: L68 here 'loss' is positive, as it should be with the phrasing; but better to stick to one numerical convention, positive or negative, and use words accordingly. It looks as though the majority of the Introduction uses positive numbers to report 'mass loss', and that is appropriate. However, it might be a bit confusing to people, since in terms of 'mass balance' these numbers should all be negative. In any case, please be consistent throughout the paper (abstract differs from main text). See L89-L100 and elsewhere.

Changes in manuscript: Wherever numbers on mass changes are shown, we now refer consistently to mass balance (negative for losses, positive for gain).

Comment: L76 change to '. . .began to accelerate and thin. . .' ('get thinner' is a bit colloquial, almost slang)

Changes in manuscript: Wording changed as proposed.

Comment: L154 'data takes' is also a bit colloquial; 'swath data' or 'data acquisitions'?

Response: Date take is a technical term, referring to the specific ground coverage of SAR strip map mode images. Therefore we keep this term.

Comment: L162, L165, L166 I think that “Raw DEMs” should be “raw DEMs” in English convention.

Response: Raw DEM is a technical term (proper name) for a specific product within the DLR DEM processing chain. Therefore we keep this term.

Comment: L173 change to ‘...data from the Antarctic Peninsula DEM. ...’

Changes in manuscript: Wording changed as proposed.

Comment: L181 ‘swaths’, not swathes (in US English at least)

Response: Swathes is OK according to dictionary.

Comment: L219 remove ‘anywhere’, and change to ‘back-slope areas’ - this is slightly confusing on first read.

Changes in manuscript: Clarified, pointing out that this refers to any slope area (L229 of revised manuscript).

Comment: L254-255 – the RMSD is somewhat high, 50 – 60 m/yr, though, a bit of a concern.

Response: Thanks for pointing this out. The comment makes clear that we did not well explain the uncertainties of the velocity data, which are specified in the details in the references cited on line 258 – 259 (same methods are used for work reported in this paper). In the Supplementary Material we added information on uncertainty estimate for the mass budget method (Section S3). The RMSD values between the TerraSAR-X and Sentinel-1 velocity products (line 254) can mainly be attributed to the different spatial resolution of the sensors. This is evident when considering the good agreement of mean velocities (0.011 m d^{-1} and -0.002 m d^{-1} for the two velocity components). The ice velocities for computing the calving fluxes are based on offset tracking using TerraSAR-X repeat pass SAR data. The uncertainty in the magnitude of the TerraSAR-X derived surface motion product at 50 m grid size is (conservatively) estimated at $\pm 0.05 \text{ m d}^{-1}$ (details in Wuite et al., 2015). We compared also GPS and TerraSAR-X velocities at five stakes on Flask and Starbuck glaciers (with flow velocities $< 1 \text{ m d}^{-1}$); the differences of velocity magnitude between GPS and the satellite product are within $\pm 0.01 \text{ m d}^{-1}$ (Supplementary Material).

Changes in manuscript: We explain that the RMSD values of TerraSAR-X and Sentinel-1 velocities are mainly due to the different spatial resolutions (L267, L268 in revised manuscript) and that velocities at flux gates are derived from TerraSAR-X images (L291, L292). The uncertainty of TerraSAR-X is specified in L254, L255.

Comment: L260 again, please change to ‘mass budget method’.

Changes in manuscript: Changed as proposed.

Comment: L297 ‘...approximately in a balanced state. ...’; Same Note for L365. L311-312 see comment re Figures 3 and 8.

Response: This statement is based on DEM differencing results, shown in the dh/dt maps and quantified in Table 1 for Larsen A and in Table 4 for Larsen B. Figures 3 and 8 (Fig. numbers of 1st manuscript version) are velocity maps and do not show mass balance.

Changes in manuscript: We added references to the relevant figures and tables in the text to make this clear (L316 for Larsen A, L402 for Larsen B).

Comment: *L510-513 – it would seem that several of the longer, thinner glaciers are evolving toward the Crane pattern of elevation change – the DBE system as well as Sjogren Glacier; and in the latest mapping, Jorum and HG are in this pattern. This is a clue / insight into how other glaciers that experience a sudden reduction in backstress at the grounding line might evolve in the future.*

Response: Thanks for pointing this out. We addressed this in L581 to L583 of the 1st manuscript version.

Comment: *Figure 2, Figure 7 – just a suggestion, make blue lines thicker, green lines thinner, to emphasize that the elevation change profile is the main point of the graphics. At first I thought the green line was binned elevation change rate (not area).*

Changes in manuscript: We changed the thickness of the lines as proposed.

Comment: *Figure 3 – This graphic might be more effective as: (a) Speed, m/d, 2016;(b) Speed, 2016-2011; and Speed, 2016-1995 – same note for Figure 8. This would highlight the slowing in recent years. Also, check, is the date for the 1995 mapping November, as written, or October, as in the following figure profiles?*

Changes in manuscript: Pronounced changes in velocity 2016 to 2011 affect only small sections of the velocity maps. We include insets in Figure 4 and Figure 9 for the main glaciers.

Comment: *Figure 4 and Figure 9 – Would it be possible to show the progression of speed versus time for the centerlines of the speed data – for example, in Figure 9, make the cross-section speed profile more narrow and place a center-line speed versus time graphic to the right of the plots?*

Changes in manuscript: We added insets displaying time series of velocities for the centre of the flux gate in Figure 5 (previous Fig. 4). In Figure 10 (previous Fig. 9) we changed the colour code so that the temporal sequence of gate velocities is clearer.

Comment: *Similarly with Figure 4. Also – please place the location of the Fig9 flux gates and the Fig4 centerlines on one of the map views. I see that they are in the Supplemental Information, along with others, but it would be good to have these few in the main text maps to go with the figures.*

Response: We checked the feasibility of displaying the flux gates and centre lines in any of the figures of the main text (maps of elevation change and velocity). The lines do not show up clearly in these figures against the colour spectrum used for velocity and elevation change. These lines show up much better in Figures S1 and S2, because the background image is bright (white/ light grey) and the maps are larger (one full page).

Anonymous Referee #2

Comment: *This manuscript presents a mass balance study for the East of the northern Antarctic Peninsula, based on remotely sensed altitude changes, and a comparison with mass changes derived from modeled surface mass balance and surface flow velocities. It is shown*

that the land-based ice is continuing to lose mass, although the rate of loss has decreased over time since the collapse of the ice shelves. The manuscript is well written and clearly structured. The different data sources are described in great detail and also the methods are clearly presented. The results for the single catchment areas are described and also provided as tables, which is quite useful. This is new data, continuing earlier observations to extend the overall record, and thus of great interest to the community. However, I would like to raise several points, which I think should be addressed before final publication:

Response: The authors would like to thank the reviewer for the constructive comments, providing very valuable support for improving the quality of the manuscript. We took into account the issues raised in the comments for revising the manuscript, as explained in the response below.

Comment 1. *In lines 272-276 error estimates for the glacier cross sections, the flow velocities and the modelled mass balance are given. They appear to come “out of the blue”. It would be good to describe how you got to these estimates.*

Response: We agree that error estimates for the mass budget method were not well explained. In the revised version of the Supplementary Material we include a new section (3.2) explaining uncertainties in flow velocity and ice thickness at the flux gates and uncertainties of surface mass balance (SMB). In the revised manuscript we add part of this information and make reference to the section in Supplementary Material.

Changes in manuscript: In L286 to L288 reference is made new section 3.2 in the Supplementary Material with uncertainty analysis for the mass budget method. Furthermore, in the revised manuscript we make clear that velocities at flux gates are exclusively derived from TerraSAR-X images (L291, L292). The uncertainty of TerraSAR-X is specified in L254, L255).

Comment 2. *There is a general estimation of ice density to be 900 kg/m^3 . This appears rather high to me, and means there is hardly any firn layer on the glaciers. There has to be an error assumption for this density value as well. This becomes important when you are concluding ice thickness from the floating glacier tongues, but also for the lowering of the surface of the grounded ice. Can there be a lowering of the surface due to firn compaction from surface melting? Maybe this could be discussed with the RACMO-results for the area. Is surface melting likely to occur on the glaciers?*

Response: For converting volume change over a certain time span to the change in mass an estimate for the change in density of the vertical snow and ice column is needed. If the mean density of the column remains unchanged the water equivalent can be obtained by multiplying the elevation change by the density of ice. Changes in density and microstructure of the firn volume would cause changes in the X-band radar backscatter coefficient. From the similarity of the radar backscatter coefficients in the 2011 and 2016 TanDEM-X images we can exclude significant changes in the structure and mean density of the snow/firn column. Furthermore, the good agreement between the IceBridge lidar based dh/dt values and the TanDEM-X based dh/dt values indicates also stability of the density and vertical structure of the snow/ice medium. Changes of density and structure would cause a vertical shift of the radar scattering phase centre within the volume, resulting in a relative shift of the surface in the SAR DEM

versus the surface in the optical data (Dall, 2007). These two features indicate that the possible error due to change of mean density of the vertical column is negligible compared to the uncertainty in dh/dt . We use a mean density of 900 kg m^{-3} which is commonly used for geodetic mass balance studies (e.g. Cogley, 2009; Haug et al., 2009). Scambos et al. (2014) use also a mean density of 900 kg m^{-3} for converting volume change into mass for their mass balance analysis of glaciers on the northern Antarctic Peninsula over the period 2001 to 2010, so that these data can be directly compared with our estimates.

The radar backscatter coefficients (σ_0) and structural patterns at the flux gates in the TerraSAR-X images correspond to typical features of glacier ice so that the density of ice can be used for computing the calving fluxes. The surface patterns and co-polarized σ_0 values (-6 dB to -9 dB) in the transition zones from grounded ice to floating ice of SCAR inlet ice shelf are indicating blue ice. Frozen firn further upstream has typical σ_0 values between -1 dB and -3 dB. The ice at the fronts of the calving glaciers is highly fractured so that corner effects cause higher σ_0 values than those of blue ice, but the structural pattern is typical for exposed glacier ice. The Landsat image of 29 October 2016 shows reduced surface reflectivity for the lower terminus section of the calving glaciers, also an indication for glacier ice.

Changes in manuscript: We added relevant information in the revised manuscript (L278 to L283) and make reference to Supplement Section 3.2 for further details.

Comment 3. *The discussion is a bit disappointing in relation to the rest of the paper, and reads like an extended (repetitive) description of the results. I think one point which could be discussed more prominent in a broader context is the connection of mass loss and sea ice (fast ice) cover in the embayments. This could be an essential contribution to a better understanding of how ice shelves form, or the stability of existing ice shelves.*

Response: Thanks for pointing this out and the suggestions. We add more substance to the discussion by referring to studies on the buttressing effects of ice mélange for calving behaviour and discussing possible impacts of recent changes in climate conditions and atmospheric circulation.

In 2013 to 2016 the fjords and bays in front of the glaciers were covered by ice mélange, whereas the wider area of the Larsen A and B embayments was covered by sea ice of different age. To illustrate these features we include in the revised Supplementary Material a TerraSAR-X image covering the proglacial fjord of Crane, Jorum and Punchbowl glaciers (Figure S4). In the discussion we refer to publications on models and observations of the buttressing effect by ice mélange affecting the seasonal advance and retreat of calving fronts of Greenland outlet glaciers (Walter et al., 2012; Todd and Christofferson, 2014; Amundson et al., 2016). Major advancements on the role of proglacial ice mélange and persistent sea ice cover for ice shelf formation would require substantial modelling work which is beyond the scope of this paper.

Changes in manuscript: Discussion on the buttressing effect of ice mélange is added in L576 to L587. Discussion on atmospheric circulation and sea ice pattern is added in L598 to L610.

Comment 4: *Figures 5 and 6: Maybe it would be better to place the labels of the catchment areas outside of them and connect with an arrow. In the form they are now they are obscuring quite a large part of the smaller catchments. The label B12 is missing, but as it's the only one maybe that's intentional.*

Changes in manuscript: We modified Figures 5 and 6 as suggested and added the missing label.

References:

- Amundson, J. M., Fahnestock, M., Truffer, M., Brown, J., Lüthi, M.P., and Motyka, R.J.: Ice mélange dynamics and implications for terminus stability, Jakobshavn Isbræ, Greenland, *J. Geophys. Res.*, 115, F01005, doi:10.1029/2009JF001405, 2016.
- Cogley, J. G.: Geodetic and direct mass-balance measurements: comparison and joint analysis, *Ann. Glaciol.*, 50, 96-100, 2009.
- Dall, J.: InSAR elevation bias caused by penetration into uniform volumes. *IEEE Trans. Geosc. Remote Sensing*, 45(7), 2319–2324, 2007.
- Haug, T., Rolstad, C., Elvehøy, H., Jackson, M., and I. Maalen-Johansen: (2009), Geodetic mass balance of the western Svartisen ice cap, Norway, in the periods 1968–1985 and 1985–2002, *Ann. Glaciol.*, 50, 119-125, 2009.
- Scambos, T. A., Berthier, E., Haran, T., Shuman, C. A., Cook, A. J., Ligtenberg, S. R. M., and Bohlander, J.: Detailed ice loss pattern in the northern Antarctic Peninsula: widespread decline driven by ice front retreats, *The Cryosphere*, 8, 2135-2145, doi:10.5194/tc-8-2135-2014, 2014.
- Walter, J. I., Jason, E., Tulaczyk, S., Brodsky, E. E., Howat, I. M., Yushin, A. H. N., and Brown, A.: Oceanic mechanical forcing of a marine-terminating Greenland glacier, *Ann. Glaciol.*, 53, 181–192, 2012.
- Todd, J. and Christoffersen, P.: Are seasonal calving dynamics forced by buttressing from ice mélange or undercutting by melting? Outcomes from full-Stokes simulations of Store Glacier, West Greenland, *The Cryosphere*, 8, 2353-2365, <https://doi.org/10.5194/tc-8-2353-2014>, 2014.

Changing pattern of ice flow and mass balance for glaciers discharging into the Larsen A and B embayments, Antarctic Peninsula, 2011 to 2016

Helmut Rott^{1,2*}, Wael Abdel Jaber³, Jan Wuite¹, Stefan Scheiblauer¹, Dana Floricioiu³, Jan Melchior van Wessem⁴, Thomas Nagler¹, Nuno Miranda⁵, Michiel R. van den Broeke⁴

[1] ENVEO IT GmbH, Innsbruck, Austria

[2] Institute of Atmospheric and Cryospheric Sciences, University of Innsbruck, Innsbruck, Austria

[3] Institute for Remote Sensing Technology, German Aerospace Center, Oberpfaffenhofen, Germany

[4] Institute for Marine and Atmospheric Research, Utrecht University, Utrecht, the Netherlands

[5] European Space Agency/ESRIN, Frascati, Italy

*Correspondence to: Helmut.Rott@enveo.at

Abstract

We analyzed volume change and mass balance of outlet glaciers on the northern Antarctic Peninsula over the periods 2011 to 2013 and 2013 to 2016, using high resolution topographic data of the bistatic interferometric radar satellite mission TanDEM-X. Complementary to the geodetic method applying DEM differencing, we computed the net mass balance of the main outlet glaciers by the ~~input/output~~mass budget method, accounting for the difference between the surface mass balance (SMB) and the discharge of ice into an ocean or ice shelf. The SMB values are based on output of the regional climate model RACMO Version 2.3p2. For studying glacier flow and retrieving ice discharge we generated time series of ice velocity from data of different satellite radar sensor, with radar images of the satellites TerraSAR-X and TanDEM-X as main source. The study area comprises tributaries to the Larsen-A, Larsen Inlet, and Prince-Gustav-Channel embayments (region A), the glaciers calving into Larsen B embayment (region B), and the glaciers draining into the remnant part of Larsen B ice shelf in SCAR Inlet (region C). The glaciers of region A, where the buttressing ice shelf disintegrated in 1995, and of region B (ice shelf break-up in 2002) show continuing losses in ice mass, with significant reduction of losses after 2013. The mass balance numbers for the grounded glacier area of the region A are ~~$B_n = -3.98 \pm 0.33 \text{ Gt a}^{-1}$~~ during 2011 to 2013 and ~~$B_n = -2.38 \pm 0.18 \text{ Gt a}^{-1}$~~ during 2013 to 2016. The corresponding numbers for region B are ~~$B_n = -5.75 \pm 0.45 \text{ Gt a}^{-1}$~~ and ~~$B_n = -2.32 \pm 0.25 \text{ Gt a}^{-1}$~~ . The mass ~~losses~~balance in region C during the two periods ~~were was modest~~slightly negative, ~~$B_n = -0.54 \pm 0.38 \text{ Gt a}^{-1}$~~ , respectively ~~$B_n = -0.58 \pm 0.25 \text{ Gt a}^{-1}$~~ . The main share in the overall mass losses of the region ~~were was~~ contributed by two glaciers: Drygalski Glacier contributing 61 % to the mass deficit of region A, and Hektor and Green glaciers accounting for 67 % to the mass deficit of region B. Hektor and Green glaciers accelerated significantly in 2010/2011, triggering elevation losses up to 19.5 m a^{-1} on the lower terminus ~~and a rate of mass depletion of 3.88 Gt a^{-1}~~ during the period 2011 to 2013, resulting in a mass balance of -3.88 Gt a^{-1} . Slowdown of calving velocities and reduced calving fluxes in 2013 to 2016 coincided with years when the ice mélange and sea ice cover ~~in front of the glaciers~~ in proglacial fjords and bays during summer.

1. Introduction

The disintegration of the ice shelves in Prince-Gustav-Channel and the Larsen A embayment in January 1995 (Rott et al., 1996) and the break-up of the northern and central sections of Larsen B embayment in March 2002 (Rack and Rott, 2004; Glasser and Scambos, 2008) triggered near-immediate acceleration of the outlet glaciers previously feeding the ice shelves, resulting in major mass losses due to increased ice discharge (Rott et al., 2002; De Angelis and Skvarca, 2003; Scambos et al., 2004; Scambos et al., 2011). Precise, spatially detailed data on flow dynamics and mass balance of these glaciers since ice-shelf disintegration are essential for understanding the complex glacier response to the loss of ice shelf buttressing, as well as to learn about processes controlling the adaptation to new boundary conditions. Furthermore, due to the complex topography of this region, spatially detailed data on glacier surface elevation change and mass balance are the key for reducing the uncertainty of northern Antarctic Peninsula (API) contributions to sea level rise.

Several studies dealt with mass balance, acceleration and thinning of glaciers after disintegration of the Larsen A and B ice shelves, with the majority focusing on glaciers of the Larsen B embayment. A complete, detailed analysis of changes in ice mass was performed by Scambos et al. (2014) for 33 glacier basins covering the API mainland and adjoining islands north of 66°S, using a combination of digital elevation model (DEM) differencing from optical stereo satellite images and repeat-track laser altimetry from the Ice, Cloud, and Land Elevation Satellite (ICESat). The DEM difference pairs cover the periods 2001-2006, 2003-2008, and 2004-2010 for different sections of the study area, and are integrated with ICESat data of the years 2003 to 2008. A detailed analysis of surface elevation change and mass depletion for API outlet glaciers draining into the Larsen-A, Larsen Inlet, and Prince-Gustav-Channel (PGC) embayments during 2011 to 2013 was reported by Rott et al. (2014), based on topographic data of the TanDEM-X/TerraSAR-X satellite formation. With an ~~annual loss in ice-a~~ mass ~~balance~~ of $-4.21 \pm 0.37 \text{ Gt a}^{-1}$ during 2011-2013 these glaciers were still largely out of balance, although the loss rate during this period was diminished by 27% compared to the loss rate reported by Scambos et al. (2014) for 2001 to 2008. Studies on frontal retreat, ice velocities, and ice discharge, based on remote sensing data of the period 1992 to 2014, are reported by Seehaus et al. (2015) for the Dinsmoor–Bombardier–Edgeworth glacier system previously feeding the Larsen A ~~ice shelf-Shelf~~ and by Seehaus et al. (2016) for glaciers of Sjögren Inlet previously feeding the PGC ice shelf.

As observed previously for Larsen A (Rott et al., 2002), the major outlet glaciers to the Larsen B embayment started to accelerate and ~~get thinner~~thin immediately after the collapse of the ice shelf (Rignot et al., 2004; Scambos et al., 2004; De Rydt et al., 2015). The patterns of acceleration,

thinning and change of frontal position have been variable in time and space. After strong acceleration during the first years, some of the main glaciers slowed down significantly after 2007, resulting in major decrease of calving fluxes. Other glaciers continued to show widespread fluctuations in velocity, with periods of major frontal retreat alternating with stationary positions or intermittent frontal advance (Wuite et al., 2015). The remnant section of Larsen B Ice Shelf in SCAR Inlet started to accelerate soon after the central and northern sections of the ice shelf broke away, triggering modest acceleration of the main glaciers flowing into the SCAR Inlet ice shelf (Wuite et al., 2015; Khazendar et al., 2015).

Several publications reported on ice export and mass balance of Larsen-B glaciers. Shuman et al. (2011) derived surface elevation change from optical stereo satellite imagery and laser altimetry of ICESat and the airborne Airborne Topographic Mapper (ATM) of NASA's IceBridge program. For the period 2001 to 2006 they report a combined ~~rate of mass losses~~ mass balance of $-8.4 \pm 1.7 \text{ Gt a}^{-1}$ for the glaciers discharging into Larsen B embayment and SCAR Inlet, excluding ice lost by frontal retreat. ICESat and ATM altimetry measurements spanning 2002–2009 show for lower Crane Glacier a period of very rapid drawdown between September 2004 and September 2005, bounded by periods of more moderate rates of surface lowering (Scambos et al., 2011). Rott et al. (2011) derived velocities and ice discharge of the nine main Larsen B glaciers in pre-collapse state (1995 and 1999) and for 2008–2009, estimating the mass ~~imbalance~~ of these glaciers in 2008 at $-4.34 \pm 1.64 \text{ Gt a}^{-1}$. Berthier et al. (2012) report a mass ~~loss rate~~ balance of $-9.04 \pm 2.01 \text{ Gt a}^{-1}$ for Larsen B glaciers, excluding SCAR Inlet, for the period 2006 to 2010/2011, based on altimetry and optical stereo imagery. Scambos et al. (2014) analysed changes in ice mass from ICESat data spanning September 2003 to March 2008 and stereo image DEMs spanning 2001/2002 to 2006. They report a combined ~~rate of mass losses~~ balance of -7.9 Gt a^{-1} for the tributaries of the Larsen B embayment and ~~of~~ -1.4 Gt a^{-1} for the tributaries to SCAR Inlet ice shelf. Wuite et al. (2015) report for main outlet glaciers strongly reduced calving fluxes during the period 2010 to 2013 compared to the first few years after ice shelf collapse.

We use high resolution data of surface topography derived from synthetic aperture radar interferometry (InSAR) satellite measurements for retrieving changes in glacier volume and estimating glacier mass balance over well-defined epochs for API outlet glaciers along the Weddell Coast between PGC and Jason Peninsula. In addition, we generate ice velocity maps to study the temporal evolution of ice motion and derive the ice discharge for the major glacier drainage basins. We compute the mass balance also by means of the ~~input-output~~ mass budget method ~~-(IOM)~~, quantifying the difference between glacier surface mass balance (SMB) and the discharge of ice into the ocean or across the grounding line to an ice shelf. The SMB estimates are obtained from

114 output of the regional atmospheric climate model RACMO Version 2.3p2 at grid size of ~ 5.5 km
115 (van Wessem et al., 2016; 2017).

116 Volume change and mass balance of glaciers discharging into the PGC, Larsen Inlet and Larsen A
117 embayments were derived by Rott et al. (2014) for the period 2011 to 2013, applying TanDEM-X
118 DEM differencing. Here we extend the observation period for the same glacier basins by covering
119 the time span 2013 to 2016. Furthermore, we present time series of surface velocity starting in
120 1993/1995 in order to relate the recent flow behavior to pre-collapse conditions.

121 For glaciers of the Larsen-B embayment we generated maps of surface elevation change by
122 TanDEM-X DEM differencing for the periods 2011 to 2013 and 2013 to 2016. From these maps we
123 derived mass changes at the scale of individual glacier drainage basins. In addition, we obtained
124 mass balance estimates for the eight main glaciers by the ~~input/output~~ mass budget method and
125 compare the results of the two independent methods. A detailed analysis of surface velocities of
126 Larsen B glaciers for the period 1995 to 2013 was presented by Wuite et al. (2015). We extend the
127 time series to cover glacier velocities up to 2016.

128 These data sets disclose large temporal and spatial variability in ice flow and surface elevation
129 change between different glacier basins and show ongoing loss of grounded ice. This provides a
130 valuable basis for studying factors responsible for instability and downwasting of glaciers and for
131 exploring possible mechanisms of adaptation to new boundary conditions.

132 **2. Data and methods**

133 **2.1 DEM differencing using TanDEM-X interferometric SAR data**

134 The study is based on remote sensing data from various satellite missions. We applied DEM
135 differencing using interferometric SAR data (InSAR) of the TanDEM-X mission to map the surface
136 elevation change and retrieve the mass balance for 24 catchments on the API east coast between
137 PGC and Jason Peninsula (Supplement, Table S1). Large glaciers are retained as single catchments
138 whereas smaller glaciers and glaciers that used to share the same outlet are grouped together. For
139 separation of glacier drainage basins inland of the frontal areas the glacier outlines of the
140 Glaciology Group, University of Swansea, are used which are available at the GLIMS data base
141 (Cook et al., 2014). We updated the glacier fronts for several dates of the study period using
142 TerraSAR-X, TanDEM-X and Landsat-8 images. Catchment outlines and frontal positions in 2011,
143 2013 and 2016 are plotted in a Landsat image of 2016-10-29 (Supplement, Figures S1 and S2).

144 The TanDEM-X mission (TDM) employs a bi-static interferometric configuration of the two
145 satellites TerraSAR-X and TanDEM-X flying in close formation (Krieger et al., 2013). The two
146 satellites form together a single-pass synthetic aperture radar (SAR) interferometer, enabling the

147 acquisition of highly accurate cross-track interferograms that are not affected by temporal
148 decorrelation and variations in atmospheric phase delay. The main objective of the mission is the
149 acquisition of a global DEM with high accuracy. The 90 % relative point-to-point height accuracy
150 for moderate terrain is ± 2 m at 12 m posting (Rossi et al., 2012; Rizzoli et al., 2012). Higher relative
151 vertical accuracy can be achieved for measuring elevation change over time.

152 Our analysis of elevation change is based on DEMs derived from interferograms acquired by the
153 TanDEM-X mission in mid-2011, -2013 and -2016. SAR data takes from descending satellite orbits,
154 acquired in 2013 and 2016, cover the API east coast glaciers between 64° S and the Jason
155 Peninsula, as well as parts of the west coast glaciers (Supplement, Figure S3). For 2011 we
156 processed data takes covering the Larsen B glaciers. Over the Larsen A glaciers TDM data from
157 2011 and 2013 had been processed in an earlier study to derive surface elevation change (SEC). The
158 mid-beam incidence angle of the various tracks varies between 36.1 and 45.6 degrees. The height of
159 ambiguity (HoA, the elevation difference corresponding to a phase cycle of 2π) varies between 20.6
160 m and 68.9 m, providing good sensitivity to elevation (Rott, 2009) (Supplement, Table S2). Only
161 track A has larger HoA and thus less height sensitivity; this track extends along the west coast and
162 covers only a very small section of study glaciers along the Weddell Coast.

163 We used the operational Integrated TanDEM-X Processor (ITP) of the German Aerospace Center
164 (DLR) to process the raw bistatic SAR data of the individual tracks into so-called Raw DEMs
165 (Rossi et al., 2012; Abdel Jaber ~~et al.~~, 2016). In the production line for the global DEM, which also
166 uses the ITP Processor, Raw DEMs are intermediate products before DEM mosaicking. An option
167 recently added to the ITP foresees the use of reference DEMs to support Raw DEM processing
168 (Lachaise and Fritz, 2016). We applied this option for generating the Raw DEMs, subtracting the
169 phase of the simulated reference DEM from the interferometric phase of the corresponding scene.
170 The recently released TanDEM-X global DEM with a posting of 0.4 arcsec was used as the main
171 ~~source for the~~ reference DEM. Although the relative elevation in output is not related to the
172 reference DEM, the presence of inconsistencies in the reference DEM may lead to artefacts in the
173 output DEM. Therefore some preparatory editing was performed: unreliable values were removed
174 based on the provided consistency mask of the global DEM and visual analysis and were substituted
175 by data ~~of from~~ the Antarctic Peninsula DEM of Cook et al. (2012). The phase difference image,
176 which has a much lower fringe frequency, is unwrapped and summed up with the simulated phase
177 image. This option provides a robust phase unwrapping performance for compiling the individual
178 DEMs. By subtracting the two DEMs and accounting for the appropriate time span we obtain a
179 surface elevation rate of change map, with horizontal posting at about 12 m x 12 m.

180 For estimating the uncertainty of the TanDEM SEC maps we use a fully independent data set

181 acquired during NASA IceBridge campaigns that became available after the production of the TDM
 182 SEC maps had been completed ([Supplement, Section S3](#)). Surface elevation rate of change data
 183 (dh/dt, product code IDHDT4) derived from Airborne Topographic Mapper (ATM) swathes,
 184 acquired on 2011-11-14 and 2016-11-10, cover longitudinal profiles on six of our study glaciers
 185 (Studinger, 2014, updated 2017). Each IDHDT4 data record corresponds to an area where two ATM
 186 lidar swathes have co-located measurements. The IDHDT4 data are provided as discrete points
 187 representing 250 m x 250 m surface area and are posted at about 80 m along-track spacing. We
 188 compare mean values of cells comprising 7 x 7 TDM dh/dt pixels (12 m x 12 m pixel size) with the
 189 corresponding IDHDT4 points. Even though the start and end dates of the TDM and ATM data sets
 190 differ by a few months, the agreement in dh/dt is very good. The root mean square differences
 191 (RMSD) of the data points range from 0.14 m a⁻¹ to 0.35 m a⁻¹ for the different glaciers, and the
 192 mean difference of the ATM – TDM data sets is dh/dt = -0.08 m a⁻¹ ([Supplement, Table S3](#)). For the
 193 error analysis we assume that the differences result from uncertainties in both data sets. The
 194 resulting RMSE for the TDM dh/dt cells is 0.20 m a⁻¹ over the five year time span, and 0.39 m a⁻¹
 195 and 0.58 m a⁻¹ for the three and two year time span, respectively.

196 In order to demonstrate the concordance of the dh/dt data sets, we show in Figure 1 a scatterplot of
 197 ATM and TDM dh/dt values from the central flowline on Crane Glacier. The TDM dh/dt data are
 198 derived from DEMs of 2011-06-30 and 2016-08-07. Because of the time shifts between ATM and
 199 TDM data acquisitions we start with the comparison 5 km inland of the front in order to avoid the
 200 impact of the shifting glacier front, of floating section of the terminus and of moving crevasse
 201 zones. The data in the figure include the points to the upper end of the ATM profile at 1000 m
 202 elevation. In spite of the time shift the agreement between the two data sets is excellent; the
 203 coefficient of determination (R²) is 0.98.

204 The agreement between the lidar and radar dh/dt data indicates that radar penetration is not an issue
 205 for deriving elevation change from the SAR based DEMs of this study. This can be attributed to the
 206 close agreement of the view angles in the corresponding SAR repeat data, acquired from the same
 207 orbit track and beam, and to the consistency of radar propagation properties in the snow and firn
 208 bodies. The latter point follows from the similarity of the backscatter coefficients of the
 209 corresponding scenes, with differences between the two dates staying below 1 dB. The radar
 210 backscatter coefficient can be used as indicator on stability ~~in~~of the structure and radar propagation
 211 properties of a snow/ice medium which determine the signal penetration and the offset of the
 212 scattering phase centre versus the surface (Rizzoli et al., 2017). The ~~TSX and~~ TDM SAR
 213 backscatter images have high radiometric accuracy (absolute radiometric accuracy 0.7 dB, relative
 214 radiometric accuracy 0.3 dB), well suitable for quantifying temporal changes in backscatter

215 (Schwerdt et al., 2010; Walter Antony et al., 2016).

216 The main outlet glaciers of the study area arise from the plateaus along the central API ice divide.
217 The plateaus stretch across elevations between about 1500 and 2000 m a.s.l. A steep escarpment,
218 dropping about 500 m in elevation, separates the plateau from the individual glacier streams and
219 cirques. The high resolution SEC maps, shown in Figures [42](#), [56](#), and [67](#), cover the areas below the
220 escarpment excluding parts of the steep rock- and ice- covered slopes along the glacier streams.
221 These gaps are due to the particular SAR observation geometry, with slopes facing towards the
222 illuminating radar beam appearing compressed (foreshortening) or being affected by superposition
223 of dual or multiple radar signals (layover) (Rott, 2009). On areas with gentle topography and on
224 slopes facing away from the radar beam (back-slopes) the surface elevation and its change can be
225 derived from the interferometric SAR images. In order to fill the gaps in areas of foreshortening and
226 layover, we checked topographic change on back-slopes. The TDM data set includes SEC data for
227 38 individual sections on back-slopes with mean slope angles ≥ 20 degrees, covering a total area of
228 787 km^2 . The mean dh/dt value of these slopes is -0.054 m a^{-1} . The satellite derived velocity maps
229 show surface velocities $< 0.02 \text{ m d}^{-1}$ ~~anywhere on the-any~~ slope areas, indicating that dynamic
230 effects are insignificant for mass turnover. This explains the observed stability of surface
231 topography.

232 There are some gaps in the SEC maps also on the plateau above the escarpment. The TDM SEC
233 analysis covers substantial parts (all together 2013 km^2) of the ice plateaus between 1500 m and
234 2000 m, the mean value dh/dt is -0.012 m a^{-1} . No distinct spatial pattern is evident. Considering the
235 small change of surface elevation in the available data samples of the ice plateau and on the slopes,
236 we assume stationary conditions for the unsurveyed slopes and the central ice plateau. For
237 estimation of uncertainty we assume for these areas a bulk uncertainty $dh/dt = \pm 0.10 \text{ m a}^{-1}$ for the
238 error budget of elevation change derived from DEMs spanning three years and $dh/dt = \pm 0.15 \text{ m a}^{-1}$
239 for DEMs spanning two years ([Supplement, Section S3](#)).

240 **2.2 Ice velocity maps and calving fluxes**

241 We generated maps of glacier surface velocity for several dates of the study period from radar
242 satellite images, extending the available velocity time series up to 2016. The main data base for the
243 recent velocity maps are repeat-pass SAR images of the satellites TerraSAR-X and TanDEM-X.
244 Gaps in these maps, primarily in the slowly moving interior, are filled with velocities derived from
245 SAR images of Sentinel-1 (S1) and of the Phased Array L-band SAR (PALSAR) on ALOS. We
246 applied offset tracking for deriving two-dimensional surface displacements in radar geometry and
247 projected these onto the glaciers surfaces defined by the ASTER-based Antarctic Peninsula digital

248 elevation model (API-DEM) of Cook et al. (2012). The velocity data set comprises the three
249 components of the surface velocity vector in Antarctic polar stereographic projection resampled to a
250 50 m grid.

251 The TerraSAR-X/TanDEM-X velocity maps are based on SAR strip map mode images of 11-day
252 repeat-pass orbits, using data spanning one or two repeat cycles. Due to the high spatial resolution
253 of the images (3.3 m along the flight track and 1.2 m in radar line-of-sight) velocity gradients are
254 well resolved. Wuite et al. (2015) estimate the uncertainty of velocity maps (magnitude) of Larsen
255 B glaciers derived from TerraSAR-X 11-day repeat pass images at $\pm 0.05 \text{ m d}^{-1}$.

256 Regarding S1 we use single look complex (SLC) Level 1 products acquired in Interferometric Wide
257 (IW) swath mode, with nominal spatial resolution 20 m x 5 m (Torres et al. 2012; Nagler et al.,
258 2015). Images of the Sentinel-1A satellite at 12-day repeat cycle cover the study region since
259 December 2014. Since September 2016 the area is also covered by the Sentinel-1B satellite,
260 providing a combined S1 data set with 6-day repeat coverage. ~~Wuite et al. (2015) estimate the~~
261 ~~uncertainty of velocity magnitude derived from TerraSAR X 11-day repeat pass images at $\pm 0.05 \text{ m}$~~
262 ~~d^{-1} .~~—In order to check the impact of combining different ice velocity products, we compared
263 TerraSAR-X/TanDEM-X velocity maps of the study area, resampled to 200 m, with S1 velocity
264 maps using data sets with a maximum time difference of 10 days. The overall mean bias (S1 –
265 TerraSAR-X/TanDEM-X) between the two data sets (sample 570,000 points) is 0.011 m d^{-1} for
266 velocity component V_e (easting) and -0.002 m d^{-1} for V_n (northing), the RMSD is 0.175 m d^{-1} for
267 V_e and 0.207 m d^{-1} for V_n . The RMSD values for the TerraSAR-X and Sentinel-1 velocity product
268 are mainly due to the different spatial resolution of the sensors. The good agreement of the mean
269 velocity values points out that velocity data from the two missions can be well merged.

270 In addition to the recently generated velocity products we use velocity data from earlier years for
271 supporting the scientific interpretation which were derived from SAR data of various satellite
272 missions, including ERS-1, ERS-2, Envisat ASAR, and ALOS PALSAR (Rott et al., 2002; 2011;
273 2014; Wuite et al., 2015).

274 In order to obtain mass balance estimates by the input/output mass budget method, we compute the
275 mass flux F across a gate of width Y [m] at the calving front or grounding line according to:

$$F_Y = \rho_i \int_0^Y [u_m(y)H(y)] dy$$

276 ρ_i is the density of ice, u_m is the mean velocity of the vertical ice column perpendicular to the gate,
277 and H is the ice thickness. We use ice density of 900 kg m^{-3} to convert ice volume into mass. From
278 the similarity of the radar backscatter coefficients in the 2011 and 2016 TanDEM-X images we can

exclude significant changes in the structure and density of the snow/firn column. The good agreement between the IceBridge lidar and the TanDEM-X dh/dt values indicates also stability of the structure and density of the snow/ice medium. Therefore the possible error due to density changes in the vertical column is negligible compared to the uncertainty in dh/dt (details in Supplement, Section S3.2). For calving glaciers full sliding is assumed across calving fronts, so that u_m corresponds to the surface velocity, u_s , obtained from satellite data. For glaciers discharging into the SCAR Inlet ice shelf we estimated the ice deformation at the flux gates applying the laminar flow approximation (Paterson, 1994). The resulting vertically averaged velocity for these glaciers is $u_m = 0.95 u_s$. The ice thickness at the flux gates is obtained from various sources. For some glaciers sounding data on ice thickness are available, measured either by in situ or airborne radar sounders (Farinotti et al., 2013; 2014; Leuschen et al. 2010, updated 2016). For glaciers with floating terminus the ice thickness is deduced from the height above sea level applying the flotation criterion.

The uncertainty estimate for mass balance at basin scale, derived by means of the mass budget method, accounts for uncertainties of surface mass balance (SMB) and for uncertainties in flow velocity and ice thickness at the flux gates (Supplement, Section S3.2). For uncertainty estimates of mass fluxes we assume $\pm 10\%$ error for the cross section area of glaciers with GPR data across or close to the gates and $\pm 15\%$ for glaciers where the ice thickness is deduced from frontal height above flotation. The velocities used for computing calving fluxes are exclusively derived from TerraSAR-X and TanDEM-X repeat pass data. For velocities across the gates we assume $\pm 5\%$ uncertainty. For surface mass balance at basin scale, based on RACMO output, the uncertainty is estimated at $\pm 15\%$.

3. Elevation change and mass balance of glaciers north of Seal Nunataks

3.1 Elevation change and mass balance by DEM differencing

The map of surface elevation change dh/dt from June/July 2013 to July/August 2016 for the glacier basins discharging into PGC, Larsen Inlet and Larsen A embayment is shown in Figure 42. The numbers on elevation change, volume change and mass balance, excluding floating glacier areas, are specified in Table 1. As explained in Section 2.1, for areas not displayed in this map (steep radar fore-slopes and the ice plateau above the escarpment) the available data indicate minimal changes in surface elevation so that stable surface topography is assumed for estimating the net mass balance.

For glaciers with major sections of floating ice and frontal advance or retreat the extent, SEC and volume change (including the subaqueous part) of the floating area and the advance/retreat area and volume are specified in Table 2. The area extent of floating ice is inferred from the reduced rate of

312 SEC compared to grounded ice, using the height above sea level as additional constraint. Dinsmoor-
313 Bombardier-Edgeworth glaciers (DBE, basin A4) had the largest floating area (56.2 km²) extending
314 about 8 km into a narrow fjord and showed also the largest frontal advance (11.7 km²) between
315 2013 and 2016.

316 The mass depletion of grounded ice in the basins A1 to A7 ($B_n = -2.38$ Gt a⁻¹) during the period
317 2013 to 2016 amounts to 60 % of the 2011 to 2013 ~~depletion rate~~value ($B_n = -3.98$ Gt a⁻¹ for the
318 grounded areas; Rott et al., 2014). The mass deficit is dominated by Drygalski Glacier ($B_n = -1.72$
319 Gt a⁻¹ for 2013 to 2016 ~~and), down from -2.18 Gt a⁻¹ for 2011 to 2013~~). A decline of mass losses
320 between the first and second period is observed for all basins except A3 (Albone, Pyke, Polaris,
321 Eliason glaciers, APPE) in Larsen Inlet which was approximately in balanced state during 2011 to
322 2016 (Table 1, Figure 2).

323 The altitude dependence of elevation change (dh/dt) for the three basins with the largest mass
324 deficit is shown in Figure 23. Positive values in the lowest elevation zone of Basin A2 and A6 are
325 due to frontal advance. The areas close to the fronts include partly floating ice so that the observed
326 SEC is smaller than on grounded areas further upstream. The largest loss rates are observed in
327 elevation zones several km inland of the front.

328 3.2 Flow velocities, calving fluxes and mass balance by the ~~input/output~~mass budget method

329 Data on flow velocities provide on one hand input for deriving calving fluxes, on the other hand
330 information for studying the dynamic response of the glaciers. Figure 3-4 shows maps of surface
331 velocities in 2011 and 2016, derived from TerraSAR-X and TanDEM-X 11-day repeat pass images,
332 and a map of the difference in velocity between October/November 1995 and 2016. Insets show the
333 velocity difference 2011 to 2016 for the main glaciers that were subject to slowdown. The 1995
334 velocity map was derived from interferometric one-day repeat pass data of crossing orbits from the
335 satellites ERS-1 and ERS-2 (map shown in Figure S3 of Rott et al., 2014, Supplementary Material).
336 In October/November 1995, ten months after ice shelf collapse, the velocities at calving fronts had
337 already accelerated significantly compared to pre-collapse conditions (Rott et al., 2002). Between
338 2011 and 2016 the flow velocities slowed down significantly. Even so, in 2016 the terminus
339 velocities of the major outlet glaciers still exceeded the November 1995 velocities.

340 Details on velocities along central flowlines of Drygalski, Edgeworth and Sjögren glaciers and the
341 position of calving fronts are shown in Figure 4-5 for different dates between 1993/1995 and 2016.
342 The distance along the x-axis refers to the 1995 grounding line retrieved from ERS-1/ERS-2 InSAR
343 data (Rott et al., 2002). The front of the three glaciers retreated since 1995 by several kilometres,

344 with the largest retreat (11 km) by Sjögren Glacier in 2012. Between 2013 and 2016 the front of
345 Edgeworth Glacier advanced by 1.5 km and the front of Sjögren Glacier by 0.5 km.

346 | ~~The velocity of Sjögren Glacier shows a gradual decrease of velocity decreased gradually~~ from 2.9
347 m d⁻¹ in August 2009 to 1.5 m d⁻¹ in October 2016, referring to the centre of the 2009 front. The
348 | ~~calving~~ velocity on Edgeworth Glacier ~~in the centre of the flux gate~~ decreased from 2.5 m d⁻¹ in
349 October 2008 to 1.1 m d⁻¹ in August 2016. The rate of deceleration between 2013 and 2016 was
350 particularly pronounced on the lowest 6 km of the terminus where the ice was ungrounded. For
351 Drygalski Glacier we show also pre-collapse velocities (January 1993), derived from 35-day ERS-1
352 repeat pass images by offset tracking. In November 1995 the glacier front was located near the pre-
353 collapse grounding line, but the flow acceleration had already propagated 10 km upstream of the
354 front. Due to rapid flow the phase of the 31 October/1 November 1995 ERS-1/ERS-2 InSAR pair is
355 decorrelated on the lowest two kilometres, prohibiting there interferometric velocity retrieval.
356 Velocities of January 1999 and November 2015 are similar, 7.0 m d⁻¹ at the location of the 2015
357 glacier front. Velocities were lower in 2007 to 2009, and higher in 2011 to 2014, reaching 8.8 m d⁻¹
358 in November 2011.

359 The recent period of abating flow velocities coincides with years when the sea ice cover persisted
360 during summer. Time series of satellite SAR images show open water in front of the glaciers during
361 several summers up to summer 2008/09 and again in the summers 2010/2011 and 2011/2012. ~~Ice~~
362 | ~~mélange and S~~ sea ice persisted all year round from winter 2012 onwards. Open leads in summer
363 and the gradual drift of ice that calved off from the glaciers indicate ~~occasional~~ moderate movement
364 of sea ice.

365 Slowdown of calving velocities is the main cause for reduced mass deficits during the period 2013
366 to 2016 compared to previous years. Numbers on calving fluxes for 2011 to 2013 and 2013 to 2016
367 | and the mass balance, derived by the ~~IOM~~ ~~mass budget method (MBM)~~, are specified for four main
368 glacier basins in Table 3. For deriving the calving flux (CF) for each period a linear interpolation
369 between the fluxes at the start date and end date of the period is applied, including a correction for
370 the time lag between ice motion and topography data. If velocity data are available on additional
371 dates in between, these are also taken into account for temporal interpolation. Whereas the SMB
372 | ~~values~~ between the periods 2011 to 2013 and 2013 to 2016 differs only by 2%, the combined annual
373 calving flux of the four glaciers is reduced by 16 % during 2013 to 2016 (Table 3). The decrease is
374 | even more pronounced when calving fluxes ~~on-of~~ individual dates in 2011, 2013 and 2016 are
375 compared. On Drygalski Glacier the calving flux decreased from 4.03 Gt a⁻¹ in November 2011 to
376 3.34 Gt a⁻¹ in December 2013 and 2.92 Gt a⁻¹ in September 2016, a decrease by 28 % during the
377 five years.

The differences in the mass balance by TDM SEC (Table 1) and ~~IOM-MBM~~ (Table3) are within the specified uncertainty. For ~~IOM-MBM~~ the mass balance of the four glaciers sums up to $B_n = -3.26 \text{ Gt a}^{-1}$ for 2011 to 2013 and $B_n = -2.23 \text{ Gt a}^{-1}$ for 2013 to 2016. The corresponding numbers from SEC analysis, after adding or subtracting the subaqueous mass changes, are $B_n = -3.01 \text{ Gt a}^{-1}$ and $B_n = -1.99 \text{ Gt a}^{-1}$ for the two periods.

For Drygalski Glacier the mass balance numbers for the two periods are $B_n = -2.29 \text{ Gt a}^{-1}$ and $B_n = -1.80 \text{ Gt a}^{-1}$ by ~~IOM-MBM~~, and versus $B_n = -2.18 \text{ Gt a}^{-1}$ and $B_n = -1.80 \text{ Gt a}^{-1}$ (including the subaqueous part) by TDM SEC analysis. The good agreement of the ~~IOM-MBM~~ and SEC mass balance values for Drygalski Glacier backs up the RACMO estimate for SMB with specific net balance $b_n = 1383 \text{ kg m}^{-2} \text{ a}^{-1}$. For the period 1980 to 2016 the mean SMB for Drygalski Glacier by RACMO is 1.35 Gt a^{-1} ($b_n = 1342 \text{ kg m}^{-2} \text{ a}^{-1}$). This is more than twice the ice mass flux across the grounding line in pre-collapse state (0.58 Gt a^{-1}) obtained as model output by Royston and Gudmundsson (2016) which would imply a highly positive mass balance taking RACMO SMB as reference for mass input. Velocity measurements in October/November 1994 at stakes on Larsen A Ice Shelf downstream of Drygalski Glacier show values that are close to the average velocity of the 10-year period 1984 to 1994 (Rott et al., 1998; Rack et al., 1999). This supports the assumption that the Larsen A tributary glaciers were approximately in balanced state before ice shelf collapse.

4. Elevation change and mass balance of Larsen B glaciers

4.1 Elevation change and mass balance by DEM differencing

The map of surface elevation change dh/dt for the glacier basins discharging into the Larsen B embayment and SCAR Inlet ice shelf is shown in Figure ~~5-6~~ for the period May/June 2011 to June/July 2013 and in Figure ~~6-7~~ for June/July 2013 to July/August 2016. The numbers on elevation change, volume change and mass balance, referring to grounded ice, are specified in Table 4 for 2011 to 2013 and in Table 5 for 2013 to 2016.

The SEC analysis shows large spatial and temporal differences in mass depletion between individual glaciers. The overall mass deficit of the Larsen B region is dominated by glaciers draining into the embayment where the ice shelf broke away in 2003 (basins B1 to B11). The annual mass ~~deficit-balance~~ of the glaciers draining into SCAR Inlet ice shelf (basins B12 to B17) ~~remained modest and was similar~~ was slightly negative in both periods: $B_n = -0.54 \text{ Gt a}^{-1}$ during 2011 to 2013 and $B_n = -0.58 \text{ Gt a}^{-1}$ during 2013 to 2016. The small glaciers (B12 to B15) were in balanced state (Table 4, Figures 6 and 7). The mass ~~balanced deficit~~ of Flask and Leppard glaciers ~~was slightly negative due to~~ can be attributed to flow acceleration and increased ice export after break-up of the main section of Larsen B Ice Shelf (Wuite et al., 2015).

411 In 2011 to 2013 the total annual net mass balance of basins B1 to B11 amounted to $B_n = -5.75 \text{ Gt a}^{-1}$,
 412 ¹, with the mass deficit dominated by Hektoria-Green (HG) glaciers ($B_n = -3.88 \text{ Gt a}^{-1}$), followed by
 413 Crane Glacier ($B_n = -0.72 \text{ Gt a}^{-1}$). The mass losses of Evans and Jorum glaciers and of basin B1
 414 (northeast of Hektoria Glacier) were also substantial, whereas the mass deficit of the other glaciers
 415 was modest. During the period 2013 to 2016 the annual mass deficit of the glacier ensemble was cut
 416 by more than half ($B_n = -2.32 \text{ Gt a}^{-1}$) compared to 2011 to 2013, with again HG dominating the
 417 ~~mass~~-loss ($B_n = -1.54 \text{ Gt a}^{-1}$). The decrease in mass depletion was also significant for other glaciers.
 418 For Crane Glacier the 2013 to 2016 ~~loss-rate~~losses ($B_n = -0.22 \text{ Gt a}^{-1}$) corresponds to only 18 % of
 419 the estimated balance flux (Rott et al., 2011), a large ~~drop~~-change since 2007 with $B_n = -3.87 \text{ Gt a}^{-1}$
 420 (Wuite et al., 2015).

421 The decline of mass depletion coincided with a period of permanent ~~sea-ice~~ cover by ice mélange
 422 and sea ice in the pro-glacial fjords and bays, starting in autumn/winter 2011. During several
 423 summers before, including summer 2010/11, the sea ice in front of the glaciers drifted away and
 424 gave way to ~~extended periods~~several weeks with open water. During the years thereafter the
 425 continuous sea ice cover obstructed the detachment of frontal ice and facilitated frontal advance.
 426 The maximum terminus advance was observed for HG glaciers, resulting in an increase of glacier
 427 area of 31.6 km^2 from 2011 to 2013 and 48.0 km^2 from 2013 to 2016 (Table 6).

428 Due to significant decrease in ice thickness the floating area on Hektoria and Green glaciers
 429 increased significantly after 2011, covering in June 2013 an area of 19.8 km^2 inland of the 2011 ice
 430 front and in June 2016 an area of 62.1 km^2 inland of the 2013 ice front, in addition to the frontal
 431 advance areas- ~~2011 to 2013, respectively 2013 to 2016~~, where the ice was almost completely
 432 ungrounded. Areas of floating ice, covering some km^2 in area, were observed on Evans Glacier and
 433 Crane Glacier, ~~increasing significantly between 2013 and 2016~~. The areas of frontal advance
 434 showed a similar temporal trend, with an increase ~~of from~~ 3.7 km^2 between 2011 and 2013 ~~and to~~
 435 5.4 km^2 between 2013 and 2016 for Evans Glacier, and 5.0 km^2 ~~and to~~ 10.5 km^2 for Crane Glacier.

436 Figure ~~7-8~~ shows the altitude dependence of elevation change (dh/dt) for four basins with large
 437 mass deficits. The largest drawdown rate (19.5 m a^{-1}) was observed on HG glaciers in the elevation
 438 zone 200 m to 300 m a.s.l. during 2011 to 2013, with substantial drawdown up to the 1000 m
 439 elevation zone. On Jorum Glacier the area affected by surface lowering extended up to 700 m
 440 elevation, with a maximum rate of 5 m a^{-1} . The drawdown pattern of Crane Glacier is different, with
 441 the zone of the largest 2011 to 2013 drawdown rates (4.5 m a^{-1}) commencing about 30 km inland of
 442 the front, extending across the elevation range 500 m to 850 m, abating and shifting further
 443 upstream in 2013 to 2016. Scambos et al. (2011) observed an anomalous drawdown pattern on the
 444 Crane terminus during the first few years after ice shelf collapse, very likely associated with

445 drainage of a subglacial lake.

446 4.2 Flow velocities, calving fluxes and mass balance by the ~~input/output~~mass budget method

447 Figure 8-9 shows maps of surface velocities in 2011 and 2016 and a map of the differences in
448 velocity between October/November 1995 and 2016. Insets show differences in velocity between
449 2011 and 2016 for HG and Crane glaciers. Gaps in the 2011 TerraSAR-X/TanDEM-X velocity map
450 are filled up with PALSAR data and in the 2016 map with Sentinel-1 data. The 1995 velocity map
451 used as reference for pre-collapse conditions, was derived from ERS one-day interferometric repeat
452 pass data. The ERS data show very little difference between 1995 and 1999 flow velocities,
453 suggesting that the glaciers were close to balanced state during those years (Rott et al, 2011). In
454 2016 the velocities of the main glaciers were still higher than in 1995, but had slowed down
455 significantly since 2011.

456 The temporal evolution of Larsen B glaciers between 1995 and 2013 is described in detail by Wuite
457 et al. (2015), showing velocity maps for 1995 and 2008-2012 and time series of velocities along
458 central flowlines of eight glaciers between 1995 and 2013. In extension, we report here velocity
459 changes since 2013 and provide details on velocities of HG and Crane glaciers in recent years,
460 including a diagram of velocities across the flux gates on different dates (Figure 910).

461 ~~The glaciers Flask and Leppard glaciers,~~ discharging into SCAR Inlet ice shelf, and the small
462 glaciers of the main Larsen B embayment (B4, B5, B8 to B11) showed only small variations in
463 velocity since 2011, though in 2016 the velocities of these glaciers were still higher than during the
464 pre-collapse period. The main glaciers were subject to significant slowdown. On Crane Glacier the
465 velocity in the centre of the flux gate decreased from a value of 6.8 m d^{-1} in July 2007 to 3.9 m d^{-1}
466 in September 2011, 2.9 m d^{-1} in November 2013 and 2.4 m d^{-1} in October 2016, still 50 % higher
467 than the velocities in 1995 and 1999. Because of major glacier thinning, the cross section of the flux
468 gate decreased significantly, so that the calving flux amounted in mid-2016 to 1.39 Gt a^{-1} , only
469 20 % larger than in 1995 to 1999. Since 2007 the drawdown rate of Crane Glacier decreased
470 steadily, from a mass balance ~~$B_H = -3.87 \text{ Gt a}^{-1}$~~ $B_H = -3.87 \text{ Gt a}^{-1}$ in June 2007 to ~~$B_H = -0.23 \text{ Gt a}^{-1}$~~ $B_H = -0.23 \text{ Gt a}^{-1}$ in November
471 2016. Also on Jorum Glacier the calving velocity decreased gradually since 2007; during 2013 to
472 2016 the glacier was close to balanced state. On the other hand the velocity at the flux gate of
473 Melville Glacier was in 2011 to 2016 only 5 % lower than in 2008, 2.6 times higher than the pre-
474 collapse velocity reported by Rott et al. (2011). This agrees with the negative mass balance by TDM
475 SEC analysis. However, the mass deficit is small in absolute terms because of the modest mass
476 turnover.

477 The velocities of Hektor and Green glaciers have been subject to significant variations since 2002,
 478 associated with major frontal retreat but also intermittent periods of frontal advance (Wuite et al.,
 479 2015). Between November 2008 and November 2009 the velocity in the centre of the Hektor flux
 480 gate increased from 1.4–7 m d⁻¹ to 2.8 m d⁻¹, slowed down slightly during 2010, and accelerated
 481 again in 2011 to reach a value of 4.2 m d⁻¹ in November 2011, followed by deceleration to 3.5 m d⁻¹
 482 in March 2012, 2.0 m d⁻¹ in July 2013 and 1.4 m d⁻¹ in June 2016 (Figure 910). Similar deceleration
 483 was observed for Green Glacier, from 4.6 m d⁻¹ in November 2011, to 2.8 m d⁻¹ in July 2013 and
 484 2.0 m d⁻¹ in June 2016.

485 The slowdown and frontal advance of Larsen B calving glaciers coincided with a period of
 486 continuous ~~sea-ice cover~~ by ice mélange and sea ice in the proglacial fjords since mid-2011,
 487 indicating significant impact of pre-frontal marine conditions on ice flow (Supplement; Figure S4).
 488 ~~We tracked~~ detached ice blocks close to glacier fronts to estimate the order of magnitude of
 489 motion. Typical values shows for for 2013 to 2016 ~~the following pre-frontal~~ displacements are: 6.1
 490 km for Crane Glacier, 2.7 km for Melville Glacier, 2.5 km for Jorum Glacier and 0.9 km for Mapple
 491 Glacier. This corresponds to about twice the flux gate velocity for Crane Glacier and about five
 492 times for Melville Glacier. The 2013 to 2016 displacement of ice blocks in front of HG glaciers (4.5
 493 km for Green, 3.9 km for Hektor) exceeded only slightly the distance of frontal advance.

494 The comparison of mass balance by ~~IOM-MBM~~ (Table 7) and SEC shows good overall agreement,
 495 as well as for most of the individual basins. The combined 2011 to 2013 annual mass balance of the
 496 five basins discharging into the main Larsen B embayment (B2, B3, B6, B7, B10) is ~~B_n = -5.26 Gt~~
 497 ~~a⁻¹~~ by TDM SEC and ~~B_n = -5.63 Gt a⁻¹~~ by ~~IOM-MBM~~, and for 2013 to 2016 ~~B_n = -2.15 Gt a⁻¹~~
 498 ~~TDM SEC~~ and ~~B_n = -2.28 Gt a⁻¹~~ by ~~IOM-MBM~~. The SEC mass balance in this comparison includes
 499 also the volume change of the floating glacier sections (Table 6). Also for Starbuck and Flask
 500 glaciers (B13, B16) the mass balance values of the two methods agree well. The only basin where
 501 the difference between the two methods exceeds the estimated uncertainty is Leppard Glacier
 502 (B17), where ~~IOM-MBM~~ (B_n = -0.89 Gt a⁻¹ and B_n -0.82 Gt a⁻¹ for the two periods) shows ~~larger~~
 503 ~~higher~~ losses than SEC (B_n = -0.21 Gt a⁻¹ and B_n -0.30 Gt a⁻¹). The SEC retrievals of the basins B3,
 504 B7, B10, B13, B16, which show good agreement between SEC and ~~IOM-MBM~~ mass balance, are
 505 based on data of the same TDM track as B17. Therefore it can be concluded that the difference in
 506 MB of Leppard Glacier is probably due to a bias either in SMB or in the cross section of the flux
 507 gate, or in both. The specific surface mass balance (Table 7) for the adjoining Flask Glacier is 39 %
 508 higher than for Leppard Glacier.

509 5. Discussion

510 The main outlet glaciers to the northern sections of Larsen Ice Shelf that disintegrated in 1995
511 (Prince-Gustav-Channel and Larsen A ice shelves, PGC-LA) and in 2002 (the main section of
512 Larsen B Ice Shelf) are still losing mass due to dynamic thinning. The losses are caused by
513 accelerated ice flow tracing back to the reduction of backstress after ice shelf break-up triggering
514 dynamic instabilities (Rott et al., 2002; 2011; Scambos et al., 2004; Wuite et al., 2015; De Rydt et
515 al., 2015; Royston and Gudmundsson, 2016).

516 On the outlet glaciers to PGC-LA (basins A1 to A7) the rate of mass depletion of grounded ice
517 decreased by 40 % ~~from the period 2011 to 2013 from ($B_n = -3.98 \pm 0.33 \text{ Gt a}^{-1}$) during to~~ the
518 period 201~~31~~ to 201~~63~~ ~~to ($B_n = -2.38 \pm 0.18 \text{ Gt a}^{-1}$) during 2013 to 2016~~. The mass deficit of the
519 area was dominated by losses of Drygalski Glacier, with an annual mass balance ~~$B_n =$~~ of -2.18 Gt a^{-1}
520 in 2011 to 2013 and ~~$B_n =$~~ -1.72 Gt a^{-1} in 2013 to 2016. Scambos et al. (2014) report for 2001 to
521 2008 a mass change balance of -5.67 Gt a^{-1} for glacier basins 21 to 25, corresponding approximately
522 to our basins A1 to A7. On Drygalski Glacier the 2003 to 2008 ~~rate of annual~~ mass ~~depletion~~
523 balance (~~$B_n =$~~ -2.39 Gt a^{-1}) by Scambos et al. (2014) was only 9 % ~~higher lower~~ than our estimate
524 for 2011 to 2013. On the other glaciers of PGC and Larsen A embayment the slow-down of calving
525 velocities and decrease in calving fluxes during the last decade was more pronounced.

526 On the outlet glaciers to Larsen B embayment (basins B1 to B11) the rate of mass depletion for
527 grounded ice decreased by 60 % ~~(from $B_n = -5.75 \pm 0.45 \text{ Gt a}^{-1}$ during 2011 to 2013, to $B_n = -2.32$~~
528 $\pm 0.25 \text{ Gt a}^{-1}$ during 2013 to 2016. Hektor and Green glaciers accounted in both periods for the
529 bulk of the mass deficit ($B_n = -3.88 \text{ Gt a}^{-1}$, $B_n = -1.54 \text{ Gt a}^{-1}$). High drawdown rates were observed
530 on HG glaciers during 2011 to 2013, with the maximum value (19.5 m a^{-1}) in the elevation zone 200
531 m to 300 m a.s.l. Our basins B1 to B11 correspond to the basins 26a and 27 to 31a of Scambos et al.
532 (2014). Based on ICESat data spanning September 2003 to March 2008 and optical stereo image
533 DEMs acquired between November 2001 to November 2006, Scambos et al. (2014) report for these
534 basins an annual mass balance ~~$B_n =$~~ of -8.39 Gt a^{-1} excluding ice lost by frontal retreat. Our rate of
535 mass loss for 2011 to 2013 amounts to 69% of this value, and for 2013 to 2016 to 36%, a similar
536 percentage decrease of mass losses as for the PGC-LA basins. After ice shelf break-up in March
537 2002 the glacier flow accelerated rapidly, causing large increase of calving fluxes during the first
538 years after Larsen B collapse, whereas on most glaciers the calving velocities slowed down
539 significantly after 2007 (Scambos et al., 2004, 2011; Rott et al., 2011; Shuman et al., 2011; Wuite at
540 al., 2015). An exception is basin B2 (HG glaciers) for which the 2011 to 2013 loss rate was 2%
541 higher than the value ($B_n = -3.82 \text{ Gt a}^{-1}$) reported by Scambos et al. (2014) for 2001 to 2008.

542 The drawdown pattern on the main glaciers shows high elevation loss rates for grounded ice shortly
543 upstream of the glacier front or upstream of the floating glacier section, and abating loss rates
544 towards higher elevation. This is the typical loss pattern for changes in the stress state at the
545 downstream end of a glacier as response to the loss of terminal floating ice (Hulbe et al., 2008). The
546 elevation change pattern of recent years is different on Crane Glacier, where elevation decline and
547 thinning migrated up-glacier during 2011 to 2016, an indication for upstream-propagating
548 disturbances (Pfeffer, 2007). Both patterns indicate that the glaciers are still away from equilibrium
549 state ~~and so that~~ dynamic thinning will continue for years.

550 We compiled surface motion and calving fluxes for main glaciers of the study region and derived
551 the surface mass balance from output of the regional atmospheric climate model RACMO. These
552 data enable to compare individual components of the mass balance. Whereas the SMB ~~differed~~
553 between the periods 2011 to 2013 and 2013 to 2016 differed only by few per cent, the calving
554 fluxes decreased significantly due to slow-down of ice motion, confirming that the mass losses were
555 of dynamic origin, an aftermath to changes in the stress regime after ice shelf collapse.

556 The terminus velocities on most glaciers are still higher than during the pre-collapse period. After
557 rapid flow acceleration during the first years after ice shelf break-up there has been a general trend
558 of deceleration afterwards, however with distinct differences in the temporal pattern between
559 individual glaciers. Glaciers with broad calving fronts show larger temporal variability of velocities
560 and calving fluxes than glaciers with small width to length ratio. In the Larsen A embayment the
561 Drygalski Glacier has been subject to major variations in flow velocity and calving flux during the
562 last decade. In 2007 to 2009 the velocity in the centre of the flux gate varied between 5.5 m d^{-1} and
563 6 m d^{-1} , increased to 8 m d^{-1} in 2011 and 2012, and decreased to 6.0 m d^{-1} in July 2016, still four
564 times higher than the velocity in 1993. In the Larsen B embayment Hektor and Green glaciers
565 showed large temporal fluctuation in velocity and a general trend of frontal retreat, but also sporadic
566 periods of frontal advance. A major intermittent acceleration event, starting in 2010, was
567 responsible for a large mass deficit in 2011 to 2013.

568 Regarding the SCAR Inlet ice shelf tributaries, the small glaciers (basin B12 to B15) were
569 approximately in balanced state, whereas Flask (B16) and Leppard (B17) glaciers ~~had showed~~ a
570 moderate mass deficit. The total mass balance of the SCAR Inlet glaciers, based on TDM SEC
571 analysis, was $B_n = -0.54 \pm 0.38 \text{ Gt a}^{-1}$ in 2011 to 2013 and $B_n = -0.58 \pm 0.38 \text{ Gt a}^{-1}$ in 2013 to 2016.
572 As for the calving glaciers to the Larsen A and B embayments, the ~~loss rate was lower~~ mass balance
573 was less negative than during the period 2001 to 2008 ($B_n = -1.37 \text{ Gt a}^{-1}$) reported by Scambos et al.
574 (2014).

575 The slowdown of flow velocities and decline in mass depletion between 2011 and 2016 coincided
576 with periods of continuous ~~sea ice cover~~age by ice mélange (a mixture of icebergs and bergy bits,
577 held together by sea ice) and sea ice in the pro-glacial fjords and bays. After several summers with
578 open water (excluding summer 2009/10 ~~when sea ice persisted~~), a period of permanent coverage by
579 ice mélange and sea ice ~~cover in front of the glaciers~~ commenced in Larsen B embayment in winter
580 2011 and in PGC and Larsen A embayment in winter 2013. Observations and modelling of seasonal
581 advance and retreat of calving fronts of Greenland outlet glaciers indicate that the buttressing
582 pressure from rigid ice mélange is principally responsible for the seasonal variations (Walter et al.,
583 2012; Todd and Christofferson, 2014; Amundson et al., 2016). Whereas for Greenland outlet
584 glaciers ice mélange usually breaks up in spring, coinciding with ice flow acceleration and
585 increased calving, the observations in the Larsen A and B embayments show persisting ice mélange
586 and sea ice cover over multiyear periods. The cold water of the surface mixed layer in the western
587 Weddell Sea favours sea ice formation and the persistence of sea ice during summer.

588 The sea ice cover impeded glacier calving, as apparent in frontal advance of several glaciers. Large
589 frontal advance was observed for HG glaciers (~3.2 km during 2011 to 2013 and ~3.8 km during
590 2013 to 2016) and Crane Glacier (~1.2 km during 2011 to 2013 and ~2.5 km during 2013 to 2016).
591 The front of Bombardier-Edgeworth glaciers advanced between 2013 and 2016 by 1.5 km and the
592 front of Sjögren Glacier by 0.5 km. The continuous sea ice cover and restricted movement of ice
593 calving off from glaciers contrasts with the rapid movement of icebergs during the first few days
594 after Larsen A and B collapse, drifting away by up to 20 km per day due to strong downslope winds
595 and local ocean currents (Rott et al., 1996; Rack and Rott 2004). For 2006 to 2015 a modest trend of
596 atmospheric cooling was observed in the study region, in particular in summer (Turner et al., 2016;
597 Oliva et al., 2017). However, this feature does not fully explain the striking difference in sea ice
598 pattern and ice drift. Changes in regional atmospheric circulation patterns affecting the frequency
599 and intensity of downslope foehn events play a main role for the presence of sea ice and the
600 variability of melt patterns (Cape et al., 2015). Clem et al. (2016) show that the interannual
601 variability of northeast Peninsula temperatures is primarily sensitive to zonal wind anomalies and
602 resultant leeside adiabatic warming. After 1999 changes in cyclonic conditions in the northern
603 Weddell Sea resulted in higher frequency of east-to-southeasterly winds, increasing the advection of
604 sea ice towards the east coast of the Antarctic Peninsula (Turner et al., 2016). Superimposed to these
605 regional patterns in atmospheric circulation are local differences in the relationship between melting
606 and foehn winds causing a comparatively high degree of spatial variability in the melt pattern
607 (Leeson et al., 2012). The break-up patterns of sea ice in summer 2017 show as well local
608 differences. Sjögren fjord and the main section of Larsen A embayment got clear of sea ice whereas

ice mélange and sea ice persisted in Larsen Inlet, the inlet in front of DBE glaciers and in the Larsen B embayment.

6. Conclusions

The analysis of surface elevation change by DEM differencing over the periods 2011 to 2013 and 2013 to 2016 shows continuing drawdown and major losses in ice mass for outlet glaciers to Prince-Gustav-Channel and the Larsen A and B embayments. During the observation period 2011 to 2016 there was a general trend of decreasing mass depletion, induced by slowdown of calving velocities resulting in reduced calving fluxes. For several glaciers frontal advance was observed in spite of ongoing elevation losses upstream. The mass balance numbers for the glaciers north of Seal Nunataks are $B_{\text{f}} = -3.98 \pm 0.33 \text{ Gt a}^{-1}$ during 2011 to 2013 and $B_{\text{f}} = -2.38 \pm 0.18 \text{ Gt a}^{-1}$ during 2013 to 2016. The corresponding numbers for glaciers calving into the Larsen B embayment for the two periods are $B_{\text{f}} = -5.75 \pm 0.45 \text{ Gt a}^{-1}$ and $B_{\text{f}} = -2.32 \pm 0.25 \text{ Gt a}^{-1}$. For the glacier discharging into SCAR Inlet ice shelf the losses were modest.

The period of decreasing flow velocities and frontal advance coincides with several years when the ice mélange and sea ice cover persisted in pro-glacial fjords during summer. Considering the ongoing mass depletion of the main glaciers and the increase of ungrounded glacier area due to thinning, we expect recurrence of periods with frontal retreat and increasing calving fluxes, in particular for those glaciers that showed major temporal variations in ice flow during the last several years.

In Larsen A embayment large fluctuations in velocity were observed for Drygalski Glacier, and in Larsen B embayment for Hektor and Green glaciers. These are the glaciers with the main share in the overall mass losses of the region: Drygalski Glacier contributed 61 % to the 2011 to 2016 mass deficit of the Larsen A/PGC outlet glaciers, and HG glaciers accounted for 67 % of the mass deficit of the Larsen B glaciers. On HG glaciers the ice flow accelerated significantly in 2010/2011, triggering elevation losses up to 19.5 m a^{-1} on the lower terminus during the period 2011 to 2013. HG glaciers have a joint broad calving front and the frontal sections are ungrounded, thus being more vulnerable to changes in atmospheric and oceanic boundary conditions than glaciers that are confined in narrow valleys.

Complementary to DEM differencing, we applied the input/output mass budget method to derive the mass balance of the main glaciers. The mass balance numbers of these two independent methods show good agreement, affirming the soundness of the reported results. The agreement backs up also the reliability of the RACMO SMB data. A strong indicator for the good quality of the TDM SEC products is the good agreement with 2011-2016 SEC data measured by the airborne laser scanner of

642 NASA IceBridge. Both data sets were independently processed. The agreement indicates that SAR
643 signal penetration does not affect the retrieval of surface elevation change on glaciers by InSAR
644 DEM differencing if repeat observation data are acquired over snow/ice media with stable
645 backscatter properties under the same observation geometry.

646

647 *Data availability.* Data sets used in this study will be made available upon publication of the final
648 version on <http://cryoportal.enveo.at/>

649 *Competing interests.* The authors declare that they have no conflict of interest.

650

651 *Acknowledgements.* The TerraSAR-X data and TanDEM-X data were made available by DLR
652 through projects HYD1864, XTI_GLAC1864, XTI_GLAC6809 and DEM_GLA1059. Sentinel- 1
653 data were obtained through the ESA Sentinel Scientific Data Hub, ALOS PALSAR data through the
654 ESA ALDEN AOALO 3741 project. Landsat 8 images, available at USGS Earth Explorer, were
655 downloaded via Libra browser. The IceBridge ATM L4 Surface Elevation Rate of Change and
656 IceBridge MCoRDS Ice Thickness version V001 data were downloaded from the NASA
657 Distributed Active Archive Center, US National Snow and Ice Data Center (NSIDC), Boulder,
658 Colorado. We wish to thank A. Cook (Univ. Swansea, UK) for providing outlines of glacier basins.
659 The work was supported by the European Space Agency, ESA Contract No. 4000115896/15/I-LG,
660 High Resolution SAR Algorithms for Mass Balance and Dynamics of Calving Glaciers (SAMBA).

661

662 **References**

663 Abdel Jaber, W.: Derivation of mass balance and surface velocity of glaciers by means of high
664 resolution synthetic aperture radar: application to the Patagonian Icefields and Antarctica, Doctoral
665 Thesis, Technical University of Munich, DLR Research Report 2016-54, 236 pp, 2016.

666 [Amundson, J. M., Fahnestock, M., Truffer, M., Brown, J., Lüthi, M.P., and Motyka, R.J.: Ice](#)
667 [mélange dynamics and implications for terminus stability, Jakobshavn Isbræ, Greenland, J.](#)
668 [Geophys. Res., 115, F01005, doi:10.1029/2009JF001405, 2016.](#)

669 Berthier, E., Scambos, T. A., and Shuman, C. A.: Mass loss of Larsen B tributary glaciers (Antarctic
670 Peninsula) unabated since 2002, Geophys. Res. Lett., 39, L13501L13501,
671 doi:10.1029/2012GL051755, 2012.

672 [Cape, M. R., Vernet, M., Skarca, P., Marinsek, S., Scambos, T., and Domack, E.: Foehn winds link](#)
673 [climate-driven warming to ice shelf evolution in Antarctica. J. Geophys. Res. Atmos., 120, 11037–](#)

11057 (doi: 10.1002/2015JD023465), 2015.

Clem, K. R., Renwick, J. A., McGregor, J. and Fogt L. R.: The relative influence of ENSO and SAM on Antarctic Peninsula climate, *J. Geophys. Res. Atmos.*, 121, 9324 – 9341, doi:10.1002/2016JD025305, 2016.

Cook, A. J., Murray, T., Luckman, A., Vaughan, D. G., and Barrand, N. E.: A new 100-m digital elevation model of the Antarctic Peninsula derived from ASTER Global DEM: Methods and accuracy assessment, *Earth Syst. Sci. Data*, 4, 129–142, doi:10.5194/essd-4-129-2012, 2012.

Cook, A. J., Vaughan, D. G., Luckman, A., and Murray, T.: A new Antarctic Peninsula glacier basin inventory and observed area changes since the 1940s, *Antarctic Science*, 26(6), 614-624, 2014.

De Rydt, J., Gudmundsson, G. H., Rott, H., and Bamber, J. L.: Modelling the instantaneous response of glaciers after the collapse of the Larsen B Ice Shelf, *Geophys. Res. Lett.*, 42(13), 5355–5363, doi: 10.1002/2015GL064355, 2015.

De Angelis, H. and Skvarca, P.: Glacier surge after ice shelf collapse, *Science*, 299 (5612), 1560–1562, doi:10.1126/science.1077987, 2003.

Farinotti, D., Corr, H. F. J., and Gudmundsson, G. H.: The ice thickness distribution of Flask Glacier, Antarctic Peninsula, determined by combining radio-echo soundings, surface velocity data and flow modelling, *Ann. Glaciol.*, 54 (63), doi:10.3189/2013AoG63A603, 2013.

Farinotti, D., King, E. C., Albrecht, A., Huss, M., and Gudmundsson, G. H.: The bedrock topography of Starbuck Glacier, Antarctic Peninsula, as measured by ground based radio-echo soundings, *Ann. Glaciol.*, 55, 22–28, 2014.

Glasser, N. F. and Scambos, T. A.: A structural glaciological analysis of the 2002 Larsen B ice-shelf collapse, *J. Glaciol.*, 54, 3–16, 2008.

Hulbe, C. L., Scambos, T. A., Youngberg, T., and Lamb, A.K.: Patterns of glacier response to disintegration of the Larsen B ice shelf, Antarctic Peninsula, *Global Planet. Change*, 63(1), 1–8, 2008.

Khazendar, A., Borstad, C. P., Scheuchl, B., Rignot, E., and Seroussi, H.: The evolving instability of the remnant Larsen B Ice Shelf and its tributary glaciers, *Earth and Planetary Science Letters*, 419(199), 2015.

Krieger, G., Zink, M., Bachmann, M., Bräutigam, B., Schulze, D., Martone, M., Rizzoli, P., Steinbrecher, U., Anthony, J. W., De Zan, F., Hajnsek, I., Papathanassiou, K., Kugler, F., Rodriguez Cassola, M., Younis, M., Baumgartner, S., Lopez Dekker, P., Prats, P., and Moreira, A.: TanDEM-X: a radar interferometer with two formation flying satellites, *Acta Astronaut.*, 89, 83–98,

doi:10.1016/j.actaastro.2013.03.008, 2013.

Lachaise, M. and Fritz, T.: Phase unwrapping strategy and assessment for the high resolution DEMs of the TanDEM-X mission, in: Proc. of IEEE Geoscience and Remote Sensing Symposium (IGARSS), 10-15 July 2016, Beijing, China, pp. 3223-3226, 2016.

Leeson, A. A., Van Wessem, J. M., Ligtenberg, S. R. M., Shepherd, A., Van den Broeke, M. R., Killick, R., Skvarca, P., Marinsek, S., and Colwell, S.: Regional climate of the Larsen B embayment 1980–2014, *Journal of Glaciology*, 63(240), 683-690. <http://doi.org/10.1017/jog.2017.39>, 2017.

Leuschen, C., Gogineni, P., Rodriguez-Morales, F., Paden, J., and Allen, C.: IceBridge MCoRDS L2 Ice Thickness, Boulder, Colorado USA. NASA National Snow and Ice Data Center Distributed Active Archive Center, doi: <http://dx.doi.org/10.5067/GDQ0CUCVTE2Q>, 2010, updated 2016.

Nagler, T., Rott, H., Hetzenecker, M., Wuite, J., and Potin, P.: The Sentinel-1 Mission: New opportunities for ice sheet observations, *Remote Sensing*, 7(7), 9371-9389; doi:10.3390/rs70709371, 2015.

Oliva, M., Navarro, F., Hrbáček, F., Hernández, A., Nývlt, D., Pereira, P., Ruiz-Fernández, J., and Trigo, R.: Recent regional climate cooling on the Antarctic Peninsula and associated impacts on the cryosphere, *Sci. Total Environ.*, 580, 210–223, doi:10.1016/j.scitotenv.2016.12.030, 2017.

Paterson, W. S. B.: *The physics of glaciers*, Third Edition, Oxford, etc., Elsevier, 1994.

Pfeffer, W. T.: A simple mechanism for irreversible tidewater glacier retreat, *J. Geophys. Res.-Earth*, 112, F03S25, doi:10.1029/2006JF000590, 2007.

Rack, W. and Rott, H.: Pattern of retreat and disintegration of Larsen B Ice Shelf, Antarctic Peninsula, *Ann. Glaciol.*, 39, 505-510, 2004.

Rack W., Rott, H., Skvarca, P., and Siegel, A.: The motion field of northern Larsen Ice Shelf derived from satellite imagery, *Ann. Glaciol.*, 29, 261-266, 1999.

Rignot, E., Casassa, G., Gogineni, P., Rivera, A., and Thomas, R.: Accelerated ice discharges from the Antarctic Peninsula following the collapse of the Larsen B Ice Shelf, *Geophys. Res. Lett.*, 31, L18401, doi:10.1029/2004GL020697, 2004.

Rizzoli, P., Bräutigam, B., Kraus, T., Martone, M., and Krieger, G.: Relative height error analysis of TanDEM-X elevation data, *ISPRS J. Photogrammet. Remote Sens.*, 73, 30–38, 2012.

Rizzoli, P., Martone, M., Rott, H., and Moreira, A.: Characterization of snow facies on the Greenland Ice Sheet observed by TanDEM-X interferometric SAR data, *Remote Sens.*, 9 (4), 315; doi:10.3390/rs9040315, 2017.

737 Rossi, C., Rodriguez Gonzalez, F., Fritz, T., Yague-Martinez, N., and Eineder, M.: TanDEM-X
 738 calibrated Raw DEM generation, *ISPRS J. Photogrammet. Remote Sens.*, 73, 12 - 20, doi:
 739 10.1016/j.isprsjprs.2012.05.014, 2012.

740 Rott, H.: Advances in interferometric synthetic aperture radar (InSAR) in earth system science,
 741 *Progress in Phys. Geogr.*, 33(6), 769-791, doi: 10.1177/0309133309350263, 2009.

742 Rott, H., Skvarca, P., and Nagler, T: Rapid collapse of Northern Larsen Ice Shelf, Antarctica,
 743 *Science*, 271, 788–792, 1996.

744 Rott H., Rack, W., Nagler, T., and Skvarca, P.: Climatically induced retreat and collapse of Northern
 745 Larsen Ice Shelf, Antarctic Peninsula, *Ann. Glaciol.*, 27, 86-92, 1998.

746 Rott, H., Rack, W., Skvarca, P., and De Angelis, H.: Northern Larsen Ice Shelf, Antarctica: Further
 747 retreat after collapse, *Ann. Glaciol.*, 34, 277– 282, 2002.

748 Rott, H., Müller, F., Nagler, T., and Floricioiu, D.: The imbalance of glaciers after disintegration of
 749 Larsen B Ice Shelf, Antarctic Peninsula, *The Cryosphere*, 5 (1), 125–134, doi:10.5194/tc-5-125-
 750 2011, 2011.

751 Rott, H., Floricioiu, D., Wuite, J., Scheiblaue, S., Nagler, T., and Kern, M.: Mass changes of outlet
 752 glaciers along the Nordenskjöld Coast, northern Antarctic Peninsula, based on TanDEM-X satellite
 753 measurements, *Geophys. Res. Lett.*, 41, doi:10.1002/2014GL061613, 2014.

754 Royston, S., and Gudmundsson, G. H.: Changes in ice-shelf buttressing following the collapse of
 755 Larsen A Ice Shelf, Antarctica, and the resulting impact on tributaries, *J. Glaciol.*, 62(235) 905–911,
 756 2016.

757 Scambos, T. A., Bohlander, J. A., Shuman, C. A., and Skvarca, P.: Glacier acceleration and thinning
 758 after ice shelf collapse in the Larsen B embayment, Antarctica, *Geophys. Res. Lett.*, 31, L18402,
 759 doi:10.1029/2004GL020670, 2004.

760 Scambos, T. A., Berthier, E., and Shuman, C. A.: The triggering of subglacial lake drainage during
 761 rapid glacier drawdown: Crane Glacier, Antarctic Peninsula, *Ann. Glaciol.*, 52(59), 74-82, 2011.

762 Scambos, T. A., Berthier, E., Haran, T., Shuman, C. A., Cook, A. J., Ligtenberg, S. R. M., and
 763 Bohlander, J.: Detailed ice loss pattern in the northern Antarctic Peninsula: widespread decline
 764 driven by ice front retreats, *The Cryosphere*, 8, 2135-2145, doi:10.5194/tc-8-2135-2014, 2014.

765 Schwerdt, M., Bräutigam, B., Bachmann, M., Döring, B., Schrank, D., Gonzalez, J. H.: Final
 766 TerraSAR-X calibration results based on novel efficient methods, *IEEE Trans. Geosc. Rem. Sens.*,
 767 48 (2), 677–689, 2010.

768 Seehaus, T., Marinsek, S., Helm, V., Skvarca, P., and Braun, M.: Changes in ice dynamics, elevation
 769 and mass discharge of Dinsmoor–Bombardier–Edgeworth glacier system, Antarctic Peninsula,
 770 Earth Planet. Sci. Lett. 427, 125–135. doi: 10.1016/j.epsl.2015.06.047, 2015.

771 Seehaus, T. C., Marinsek, S., Skvarca, P., van Wessem, J. M., Reijmer, C. H., Seco, J. L., and Braun,
 772 M. H.: Dynamic response of Sjögren Inlet glaciers to ice shelf breakup - a remote sensing data
 773 analysis, Front. Earth Sci. 4:66, doi: 10.3389/feart.2016.00066, 2016.

774 Shuman, C. A., Berthier, E., and Scambos, T. A.: 2001–2009 elevation and mass losses in the
 775 Larsen A and B embayments, Antarctic Peninsula, J. Glaciol., 57, 737–754, 2011.

776 Studinger, M. S: IceBridge ATM L4 Surface Elevation Rate of Change, Version 1, Subset M699,
 777 S10, NASA Distributed Active Archive Center, National Snow and Ice Data Center, Boulder,
 778 Colorado USA, 2014, updated 2017, doi: <http://dx.doi.org/10.5067/BCW6CI3TXOCY>, [Accessed
 779 25 July 2017].

780 Todd, J. and Christoffersen, P.: Are seasonal calving dynamics forced by buttressing from ice
 781 mélange or undercutting by melting? Outcomes from full-Stokes simulations of Store Glacier, West
 782 Greenland, The Cryosphere, 8, 2353-2365, <https://doi.org/10.5194/tc-8-2353-2014>, 2014.

783 Torres, R., Snoeij, P., Geudtner, D., Bibby, D., Davidson, M., Attema, E., Potin, P., Rommen, B.,
 784 Floury, N., Brown, M., Navas Travera, I., Deghaye, P., Duesmann, B., Rosich, B., Miranda, N.,
 785 Bruno, C., L'Abbate, M., Croci, R., Pietropaolo, A., Huchler, M., Rostan, F.: GMES Sentinel-1
 786 mission, Remote Sens. Environ., 120, 9–24, 2012.

787 Turner, J., Lu, H., White, I., King, J. C., Phillips, T., Hosking, J. S., Bracegirdle, T. J., Marshall, G.
 788 J., Mulvaney, R. and Deb, P.: Absence of 21st century warming on Antarctic Peninsula consistent
 789 with natural variability, Nature, 535, 411–415, doi:10.1038/nature18645, 2016.

790 van Wessem, J. M., Ligtenberg, S. R. M., Reijmer, C. H., van de Berg, W. J., van den Broeke, M.
 791 R., Barrand, N. E., Thomas, E. R., Turner, J., Wuite, J., Scambos, T. A., and van Meijgaard, E.: The
 792 modelled surface mass balance of the Antarctic Peninsula at 5.5 km horizontal resolution, The
 793 Cryosphere, 10, 271-285, 2016.

794 van Wessem, J. M., van de Berg, W. J., Noël, B. P. Y., van Meijgaard, E., Birnbaum, G., Jakobs, C.
 795 L., Krüger, K., Lenaerts, J. T. M., Lhermitte, S., Ligtenberg, S. R. M., Medley, B., Reijmer, C. H.,
 796 van Tricht, K., Trusel, L. D., van Ulf, L. H., Wouters, B., Wuite, J., and van den Broeke, M. R.:
 797 Modelling the climate and surface mass balance of polar ice sheets using RACMO2, part 2:
 798 Antarctica (1979–2016), The Cryosphere Discuss., <https://doi.org/10.5194/tc-2017-202>, in review,
 799 2017.

800 Walter Antony, J. M., Schmidt, K., Schwerdt, M., Polimeni, D., Tous Ramon, N., Bachmann M.,
801 and Gabriel Castellanos, A.: Radiometric accuracy and stability of TerraSAR-X and TanDEM-X,
802 Proceedings of the European Conference on Synthetic Aperture Radar (EUSAR), 6 – 9 June 2016,
803 Hamburg, Germany.

804 [Walter, J. I., Jason, E., Tulaczyk, S., Brodsky, E. E., Howat, I. M., Yushin, A. H. N., and Brown, A.:](#)
805 [Oceanic mechanical forcing of a marine-terminating Greenland glacier, Ann. Glaciol., 53, 181–192,](#)
806 [2012.](#)

807 Wuite, J., Rott, H., Hetzenecker, M., Floricioiu, D., De Rydt, J., Gudmundsson, G. H., Nagler, T.,
808 and Kern, M.: Evolution of surface velocities and ice discharge of Larsen B outlet glaciers from
809 1995 to 2013, The Cryosphere, 9, 957-969, doi:10.5194/tc-9-957-2015, 2015.

810

811 Tables

812 **Table 1.** Rates of surface elevation change, volume change and mass balance by means of TDM
813 DEM differencing 2013 to 2016, for glacier basins discharging into Prince-Gustav-Channel, Larsen
814 Inlet and Larsen A embayment. dh/dt is the mean rate of elevation change of the area covered by
815 the high resolution map (Fig. 42). The basin area refers to ice front positions delineated in
816 TanDEM-X images of 2016-07-16, 2016-07-27, 2016-08-18. The rates of ice volume change
817 (dV/dt) and total mass balance (dM/dt) refer to grounded ice. * dM/dt 2011-2013 for grounded areas
818 of basins A1 to A7 from the TDM SEC analysis by Rott et al., (2014).

| ID | Basin name | Basin area [km ²] | dh/dt map [km ²] | dh/dt [m a ⁻¹] | dV/dt [km ³ a ⁻¹] | Uncertainty [km ³ a ⁻¹] | dM/dt [Gt a ⁻¹] 2013-16 | * dM/dt [Gt a ⁻¹] 2011-13 |
|----|------------------------|-------------------------------|--------------------------------|------------------------------|--|--|---------------------------------------|---|
| A1 | Cape Longing Peninsula | 668.9 | 576.9 | -0.257 | -0.146 | ±0.041 | -0.131 | -0.150 |
| A2 | Sjögren-Boydell (SB) | 527.6 | 188.0 | -1.239 | -0.241 | ±0.046 | -0.217 | -0.364 |
| A3 | APPE glaciers | 513.6 | 231.9 | -0.137 | -0.032 | ±0.052 | -0.029 | +0.056 |
| A4 | DBE glaciers | 653.9 | 194.3 | -0.286 | -0.063 | ±0.058 | -0.057 | -0.396 |
| A5 | Sobral Peninsula | 257.9 | 198.5 | -0.173 | -0.034 | ±0.018 | -0.031 | -0.145 |
| A6 | Cape Worsley coast | 625.1 | 291.4 | -0.742 | -0.217 | ±0.051 | -0.195 | -0.800 |
| A7 | Drygalski Glacier | 998.3 | 604.7 | -3.187 | -1.913 | ±0.074 | -1.722 | -2.179 |
| | <i>Total</i> | 4245.3 | 2285.7 | | -2.646 | ±0.199 | -2.382 | -3.978 |

819

820 **Table 2.** (a) Area extent of floating ice in 2016; (b) and (c) rate of surface elevation change and
821 volume change 2013 to 2016 of floating ice (a, b, c excluding the areas of frontal advance); (d) and
822 (e) extent and volume of frontal advance (+) or retreat (-) areas.

| ID | Basin name | (a) Floating area [km ²] | (b) Mean dh/dt [m a ⁻¹] | (c) Mean dV/dt [km ³ a ⁻¹] | (d) Advance/ retreat area [km ²] | (e) Volume [km ³] |
|----|--------------------|--------------------------------------|---------------------------------------|---|--|-------------------------------|
| A2 | Sjögren-Boydell | 6.09 | +1.250 | 0.062 | +1.96 | +0.403 |
| A4 | DBE glaciers | 56.22 | +0.131 | 0.060 | +11.74 | +2.017 |
| A6 | Cape Worsley coast | 4.89 | +0.194 | 0.008 | +2.92 | +0.550 |
| A7 | Drygalski Glacier | 4.57 | -2.231 | -0.082 | -1.40 | -0.360 |

823

Table 3. Mean specific surface mass balance, b_n , for 2011 to 2016, and rates of surface mass balance (SMB), calving flux (CF) and mass balance by ~~IOM~~ the mass budget method (MB) in Gt a^{-1} for the periods 2011 to 2013 and 2013 to 2016 for outlet glaciers north of Seal Nunataks.

| ID | Glacier | b_n 11-16 $\text{kg m}^{-2}\text{a}^{-1}$ | SMB 2011- 13 Gt a^{-1} | SMB 2013- 16 Gt a^{-1} | CF 2011- 13 Gt a^{-1} | CF 2013- 16 Gt a^{-1} | MB 2011 -13 Gt a^{-1} | MB 2013 -16 Gt a^{-1} |
|----|-----------|--|------------------------------------|------------------------------------|-----------------------------------|-----------------------------------|-----------------------------------|-----------------------------------|
| A2 | SB | 653 | 0.314 | 0.362 | 0.861 | 0.673 | -0.547±0.144 | -0.311±0.119 |
| A3 | APPE | 903 | 0.446 | 0.470 | 0.517 | 0.488 | -0.071±0.088 | -0.018±0.089 |
| A4 | DBE | 982 | 0.624 | 0.646 | 0.980 | 0.748 | -0.356±0.181 | -0.102±0.153 |
| A7 | Drygalski | 1383 | 1.398 | 1.374 | 3.687 | 3.177 | -2.289±0.619 | -1.803±0.544 |

Table 4. Rate of surface elevation change for areas by means of TDM DEM differencing 2011 to 2013 for glacier basins of the Larsen B embayment. dh/dt is the mean rate of elevation change of the area covered by the high resolution map (Fig. 56). The basin area refers to ice front positions delineated in TanDEM-X images of 2013-06-20 and 2013-07-01. The rates of ice volume change (dV/dt) and total mass balance (dM/dt) refer to grounded ice.

| ID | Basin name | Total basin area [km^2] | TDM surveyed area [km^2] | Mean dh/dt [m a^{-1}] | dV/dt [$\text{km}^3 \text{a}^{-1}$] | Uncertainty [$\text{km}^3 \text{a}^{-1}$] | dM/dt [Gt a^{-1}] |
|-----|-------------------------|---------------------------------------|---|--|--|--|-----------------------------------|
| B1 | West of SN | 638.1 | 494.1 | -0.693 | -0.342 | ±0.063 | -0.308 |
| B2 | Hektoria Green | 1167.5 | 491.8 | -8.844 | -4.312 | ±0.145 | -3.881 |
| B3 | Evans | 266.9 | 137.3 | -2.700 | -0.364 | ±0.032 | -0.328 |
| B4 | Evans Headland | 117.7 | 106.8 | -0.476 | -0.051 | ±0.011 | -0.046 |
| B5 | Punchbowl | 119.9 | 84.2 | -0.761 | -0.064 | ±0.013 | -0.058 |
| B6 | Jorum | 460.3 | 110.6 | -2.157 | -0.239 | ±0.063 | -0.215 |
| B7 | Crane | 1322.6 | 343.8 | -2.318 | -0.805 | ±0.179 | -0.724 |
| B8 | Larsen B coast | 142.6 | 95.8 | -0.085 | -0.046 | ±0.016 | -0.041 |
| B9 | Mapple | 155.4 | 92.4 | -0.524 | -0.048 | ±0.018 | -0.043 |
| B10 | Melville | 291.5 | 139.9 | -0.859 | -0.120 | ±0.036 | -0.108 |
| B11 | Pequod | 150.3 | 115.1 | +0.025 | +0.003 | ±0.015 | +0.003 |
| | <i>Total B1 to B11</i> | <i>4832.9</i> | <i>2211.6</i> | | <i>-6.388</i> | <i>±0.495</i> | <i>-5.749</i> |
| B12 | Rachel | 51.8 | 38.9 | -0.046 | -0.002 | ±0.006 | -0.002 |
| B13 | Starbuck | 299.4 | 169.4 | -0.118 | -0.020 | ±0.035 | -0.018 |
| B14 | Stubb | 108.3 | 87.9 | +0.116 | -0.001 | ±0.011 | -0.001 |
| B15 | SCAR IS coast | 136.8 | 102.4 | -0.184 | -0.019 | ±0.014 | -0.017 |
| B16 | Flask | 1130.6 | 516.3 | -0.629 | -0.325 | ±0.138 | -0.292 |
| B17 | Leppard | 1851.0 | 946.5 | -0.243 | -0.230 | ±0.219 | -0.207 |
| | <i>Total B12 to B17</i> | <i>3577.9</i> | <i>1861.4</i> | | <i>-0.597</i> | <i>±0.423</i> | <i>-0.537</i> |

832 **Table 5.** Rate of surface elevation change for areas by means of TDM DEM differencing 2013 to
833 2016 for glacier basins of the Larsen B embayment. dh/dt is the mean rate of elevation change of
834 the area covered by the high resolution map (Fig. 67). The basin area refers to ice front positions
835 delineated in TanDEM-X images of 2016-06-27 and 2016-08-01. The rates of ice volume change
836 (dV/dt) and total mass balance (dM/dt) refer to grounded ice.

| ID | Basin name | Total basin area [km ²] | TDM surveyed area [km ²] | Mean dh/dt [m a ⁻¹] | dV/dt [km ³ a ⁻¹] | Uncertainty [km ³ a ⁻¹] | dM/dt [Gt a ⁻¹] |
|-----|-------------------------|-------------------------------------|--------------------------------------|-----------------------------------|--|--|-------------------------------|
| B1 | West of SN | 638.7 | 485.6 | -0.172 | -0.084 | ±0.043 | -0.076 |
| B2 | Hektoria Green | 1215.7 | 552.8 | -3.092 | -1.708 | ±0.099 | -1.538 |
| B3 | Evans | 272.3 | 165.3 | -1.494 | -0.238 | ±0.021 | -0.214 |
| B4 | Evans Headland | 117.7 | 106.8 | -0.331 | -0.035 | ±0.007 | -0.032 |
| B5 | Punchbowl | 119.9 | 84.2 | -0.488 | -0.041 | ±0.009 | -0.037 |
| B6 | Jorum | 461.4 | 111.7 | -0.989 | -0.110 | ±0.042 | -0.099 |
| B7 | Crane | 1333.4 | 354.0 | -0.753 | -0.247 | ±0.120 | -0.222 |
| B8 | Larsen B coast | 142.6 | 96.0 | -0.166 | -0.016 | ±0.011 | -0.014 |
| B9 | Mapple | 155.4 | 92.8 | -0.240 | -0.022 | ±0.012 | -0.020 |
| B10 | Melville | 292.9 | 140.9 | -0.584 | -0.081 | ±0.024 | -0.073 |
| B11 | Pequod | 150.6 | 115.3 | +0.069 | 0.008 | ±0.011 | +0.007 |
| | <i>Total B1 to B11</i> | <i>4900.2</i> | <i>2305.5</i> | | <i>-2.574</i> | <i>±0.335</i> | <i>-2.318</i> |
| B12 | Rachel | 51.8 | 38.9 | +0.040 | 0.002 | ±0.004 | +0.002 |
| B13 | Starbuck | 299.4 | 169.4 | +0.006 | 0.001 | ±0.023 | +0.001 |
| B14 | Stubb | 108.3 | 87.9 | +0.115 | 0.010 | ±0.007 | +0.009 |
| B15 | SCAR IS coast | 136.8 | 102.4 | -0.087 | -0.009 | ±0.009 | -0.008 |
| B16 | Flask | 1130.6 | 516.3 | -0.604 | -0.312 | ±0.092 | -0.281 |
| B17 | Leppard | 1851.0 | 946.5 | -0.345 | -0.337 | ±0.146 | -0.303 |
| | <i>Total B12 to B17</i> | <i>3577.9</i> | <i>1861.5</i> | | <i>-0.645</i> | <i>±0.281</i> | <i>-0.580</i> |

837
838
839

840 **Table 6.** (a) Area extent of floating ice in 2013 (A) and 2016 (B); (b) and (c) rate of surface
841 elevation change and volume change 2011 to 2013 (A) and 2013 to 2016 (B) of floating ice ([a](#), [b](#), [c](#)
842 ~~excluding~~ the areas of frontal advance); (d) and (e) extent and volume of frontal advance areas.

| ID | Basin name | (a) Floating area [km ²] | (b) Mean dh/dt [m a ⁻¹] | (c) Mean dV/dt [km ³ a ⁻¹] | (d) Advance area [km ²] | (e) Volume [km ³] |
|------------------------|------------|--|---|---|---|----------------------------------|
| (A) 2011 - 2013 | | | | | | |
| B2 | HG | 19.81 | -1.920 | -0.308 | 31.65 | 11.676 |
| B3 | Evans | 5.55 | -1.264 | -0.057 | 3.66 | 0.807 |
| B6 | Jorum | 0.40 | +3.510 | +0.011 | 0.54 | 0.134 |
| B7 | Crane | 2.01 | +3.770 | +0.061 | 4.96 | 2.164 |
| (B) 2013 - 2016 | | | | | | |
| B2 | HG | 62.09 | -0.002 | -0.001 | 47.96 | 11.270 |
| B3 | Evans | 14.56 | -0.652 | -0.077 | 5.39 | 0.931 |
| B6 | Jorum | 1.15 | +0.305 | +0.003 | 0.78 | 0.165 |
| B7 | Crane | 7.99 | -2.620 | -0.169 | 10.54 | 3.301 |
| B10 | Melville | 0.88 | -0.966 | -0.007 | 1.20 | 0.219 |

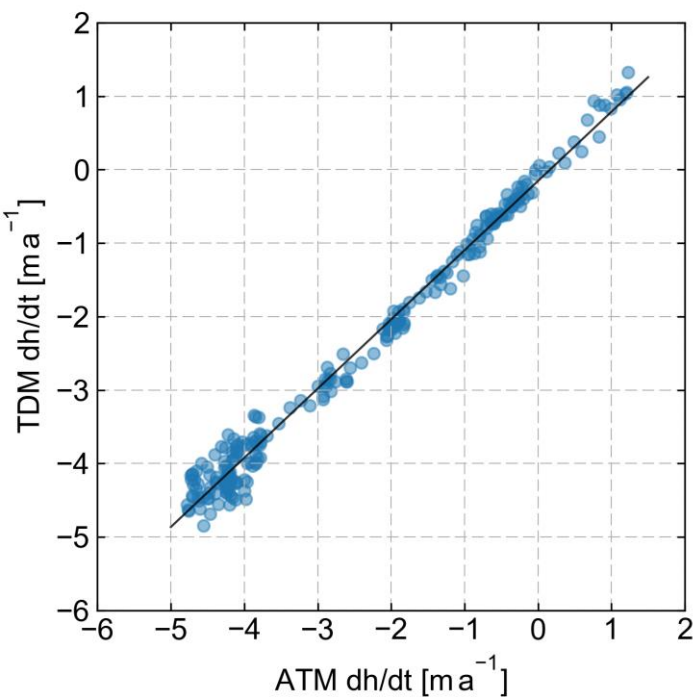
843

844 **Table 7.** Mean specific surface mass balance (b_n) 2011-2016, annual surface mass balance (SMB)
845 and calving flux (CF) 2011-2013 and 2013-2016, and resulting ~~IOM~~-mass balance (MB) in Gt a⁻¹
846 for Larsen B glaciers.

| ID | Glacier | b_n 11-16 kg m ⁻² a ⁻¹ | SMB 2011- 13 Gt a ⁻¹ | SMB 2013- 16 Gt a ⁻¹ | CF 2011- 13 Gt a ⁻¹ | CF 2013- 16 Gt a ⁻¹ | MB 2011 -13 Gt a ⁻¹ | MB 2013 -16 Gt a ⁻¹ |
|-----|----------|---|------------------------------------|------------------------------------|-----------------------------------|-----------------------------------|-----------------------------------|-----------------------------------|
| B2 | HG | 1400 | 1.563 | 1.644 | 5.733 | 3.389 | -4.170±0.936 | -1.745±0.590 |
| B3 | Evans | 562 | 0.137 | 0.156 | 0.389 | 0.304 | -0.252±0.065 | -0.148±0.053 |
| B6 | Jorum | 884 | 0.376 | 0.427 | 0.457 | 0.361 | -0.081±0.092 | +0.066±0.86 |
| B7 | Crane | 837 | 1.023 | 1.159 | 2.093 | 1.565 | -1.070±0.280 | -0.406±0.247 |
| B10 | Melville | 330 | 0.091 | 0.100 | 0.146 | 0.144 | -0.055±0.021 | -0.044±0.022 |
| B13 | Starbuck | 287 | 0.078 | 0.091 | 0.067 | 0.068 | +0.011±0.014 | +0.023±0.016 |
| B16 | Flask | 693 | 0.722 | 0.824 | 1.085 | 1.118 | -0.363±0.163 | -0.294±0.176 |
| B17 | Leppard | 500 | 0.874 | 0.961 | 1.760 | 1.780 | -0.886±0.237 | -0.819±0.246 |

847

848



851
852 **Figure 1.** Scatterplot of measurements of surface elevation change (dh/dt) 2016 - 2011 on the
853 central flowline of Crane Glacier based on IceBridge ATM and TanDEM-X elevation data. The line
854 shows the linear fit.

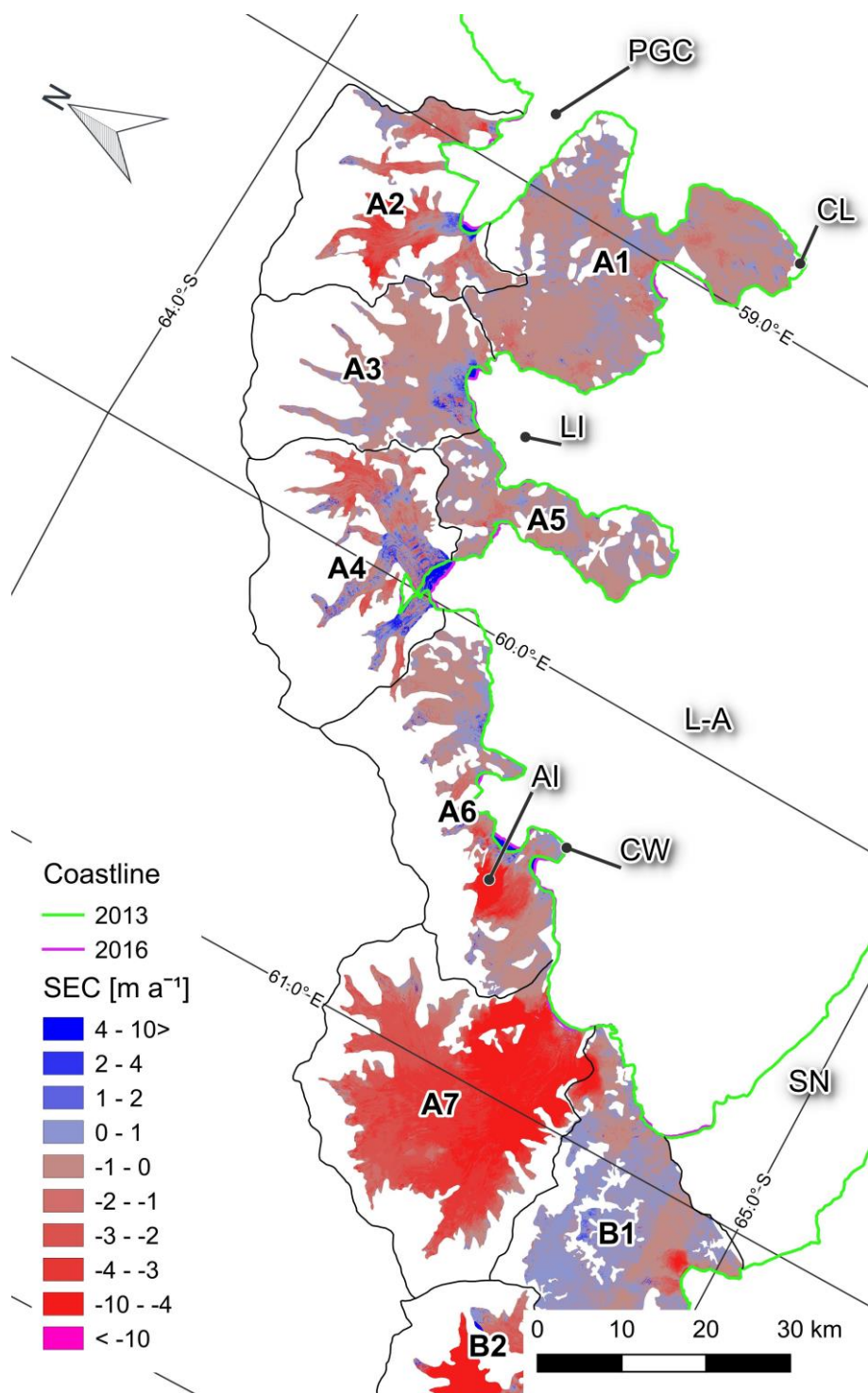


Figure 12. Map of surface elevation change dh/dt (m a^{-1}) June/July 2013 to July/August 2016 on glaciers north of Seal Nunataks (SN). AI – Arrol Icefall, CL – Cape Longing, CW – Cape Worsley, L-A – Larsen A embayment, LI – Larsen Inlet, PGC – Prince-Gustav-Channel.

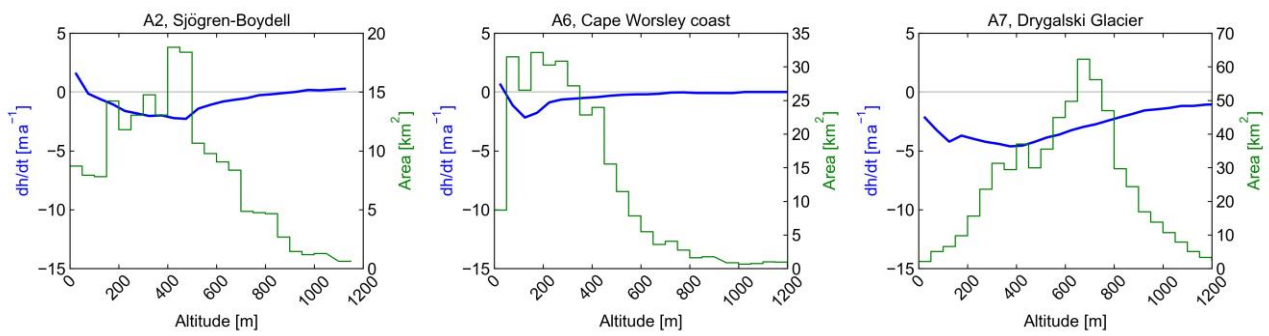


Figure 23. Rate of glacier surface elevation change dh/dt (in $m a^{-1}$) 2013 to 2016 versus altitude in 50 m intervals for basins A2, A6 and A7. Green line: hypsometry of surveyed glacier area in km^2 .

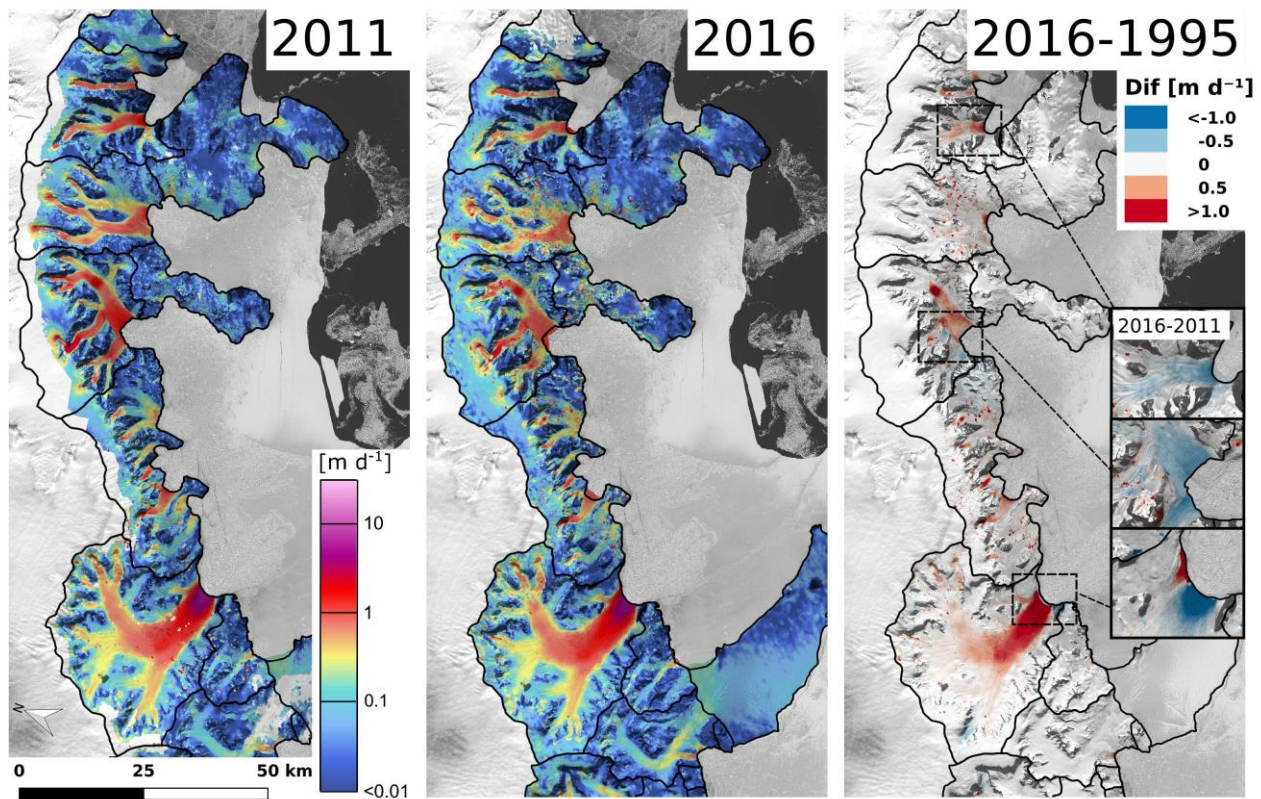


Figure 34. Magnitude of ice velocity [$m d^{-1}$] 2011 and 2016 derived from TerraSAR-X and TanDEM-X data. Gaps in 2011 filled with PALSAR data and in 2016 filled with Sentinel-1 data. Right: Map of velocity difference 2016 minus 1995 (October/November). Insets: velocity difference 2016 minus 2011 for Sjögren, DBE and Drygalski glaciers.

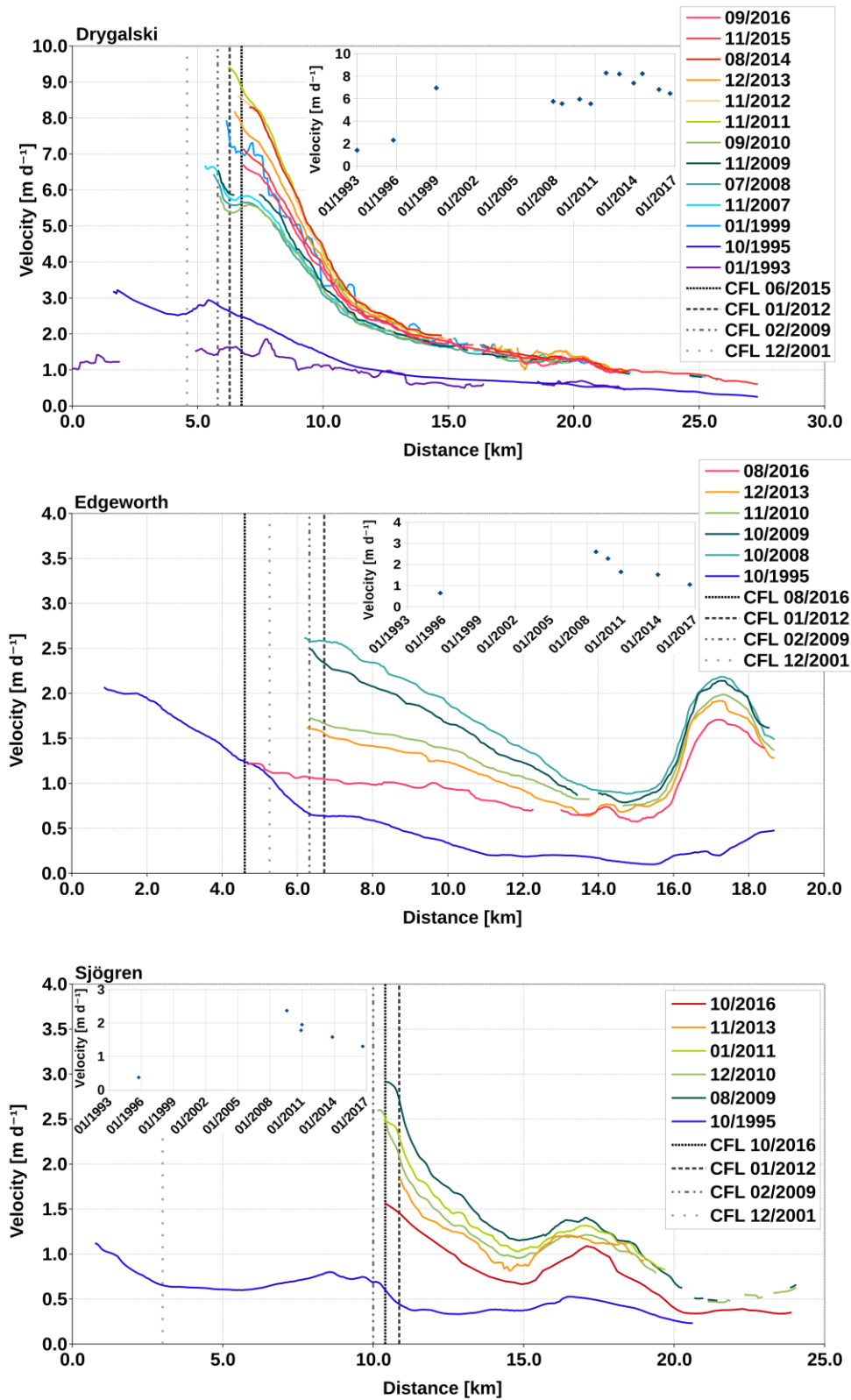
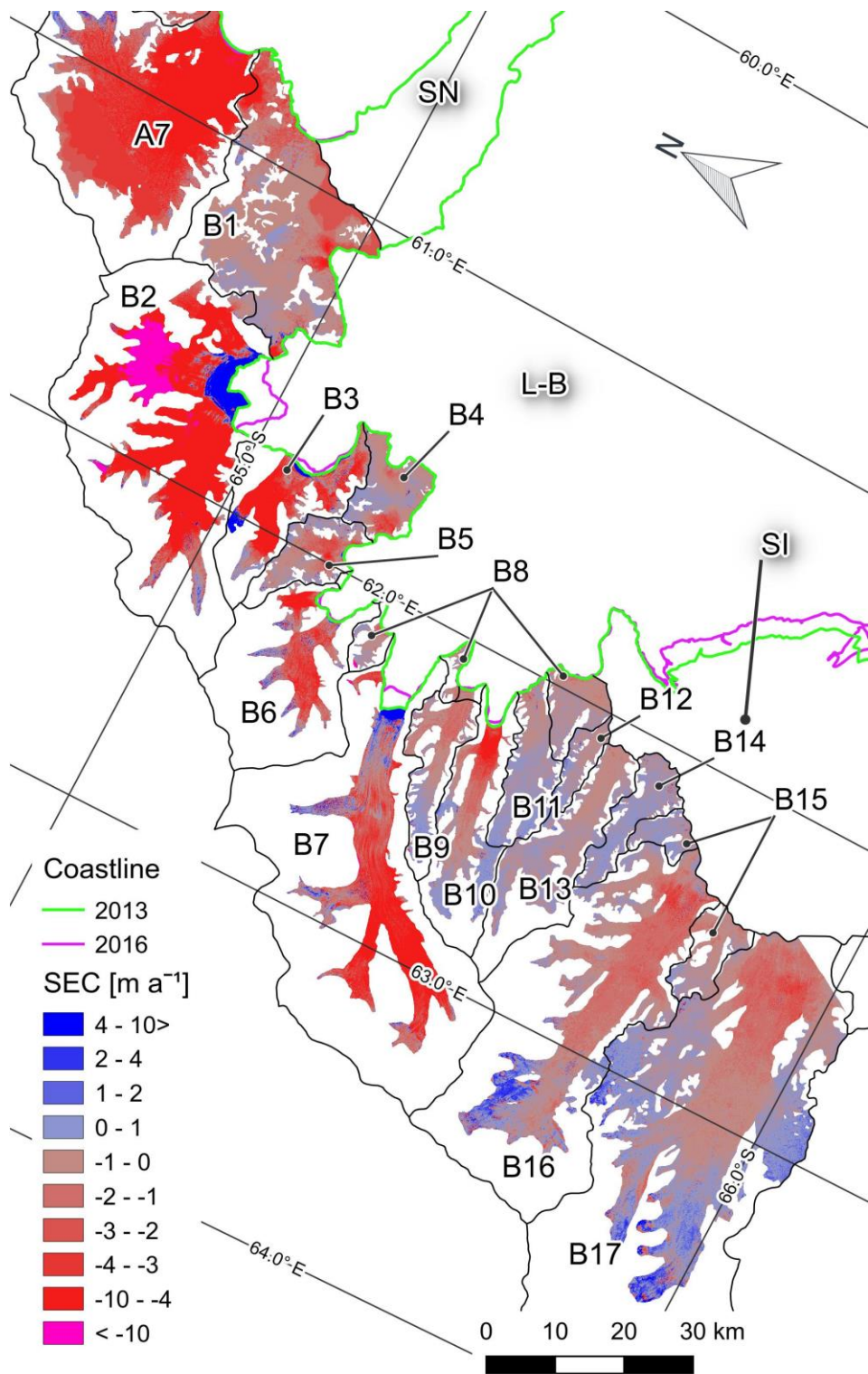


Figure 5. Surface velocities along the central flow lines of Drygalski, Edgeworth and Sjögren glaciers and their frontal positions on different dates (month/year). The x- and y-scales are different for individual glaciers. Vertical lines show positions of the calving front. The insets show velocities in the centre of the flux gates.



876

877 **Figure 56.** Map of surface elevation change (SEC m a^{-1}) May/June 2011 to June/July 2013 on
878 glaciers of Larsen B embayment (L-B). SN – Seal Nunataks. SI -SCAR Inlet ice shelf.

879

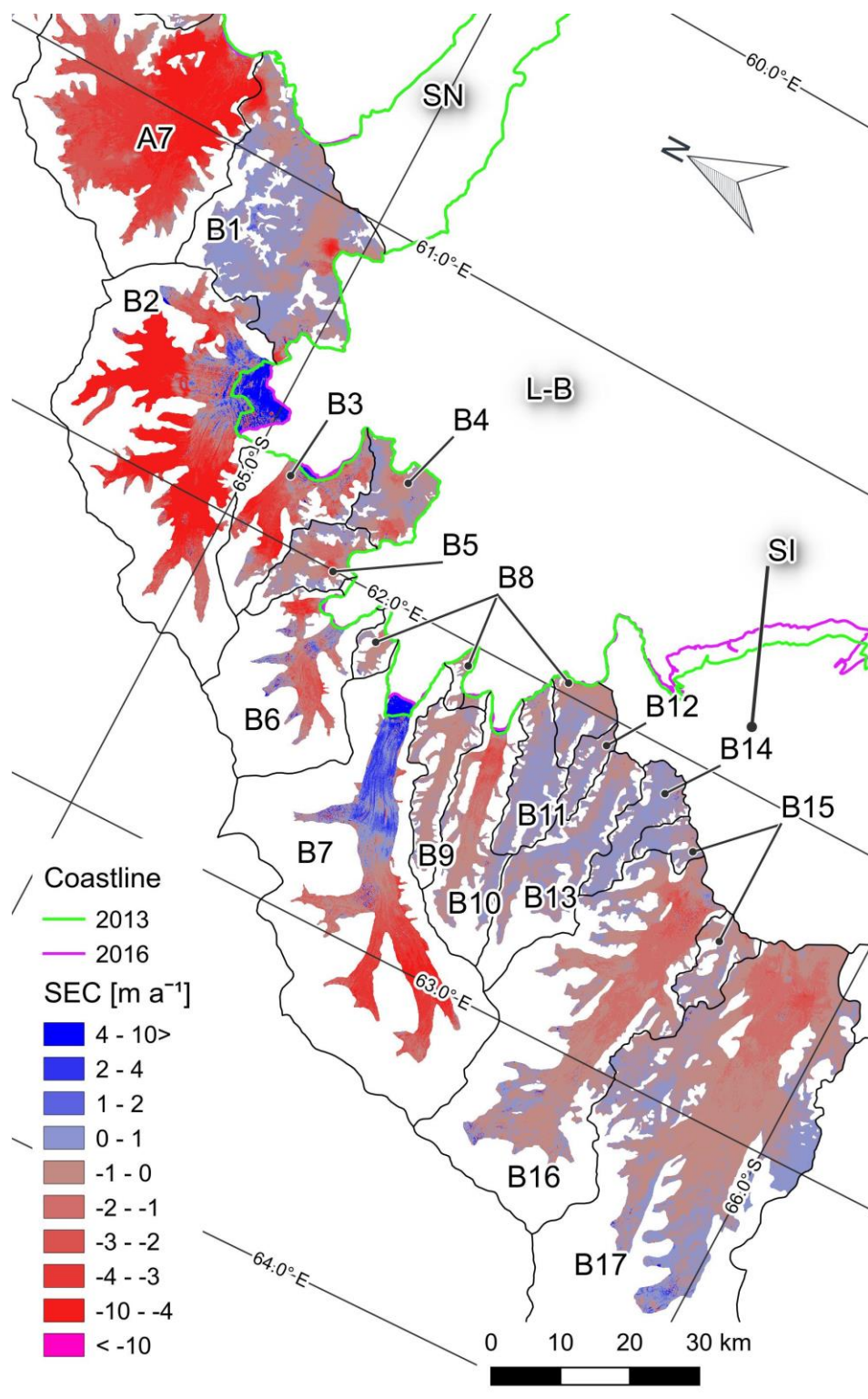


Figure 67. Map of surface elevation change (SEC m a^{-1}) June/July 2013 to July/August 2016 on glaciers of Larsen B embayment (L-B). SN – Seal Nunataks. SI -SCAR Inlet ice shelf.

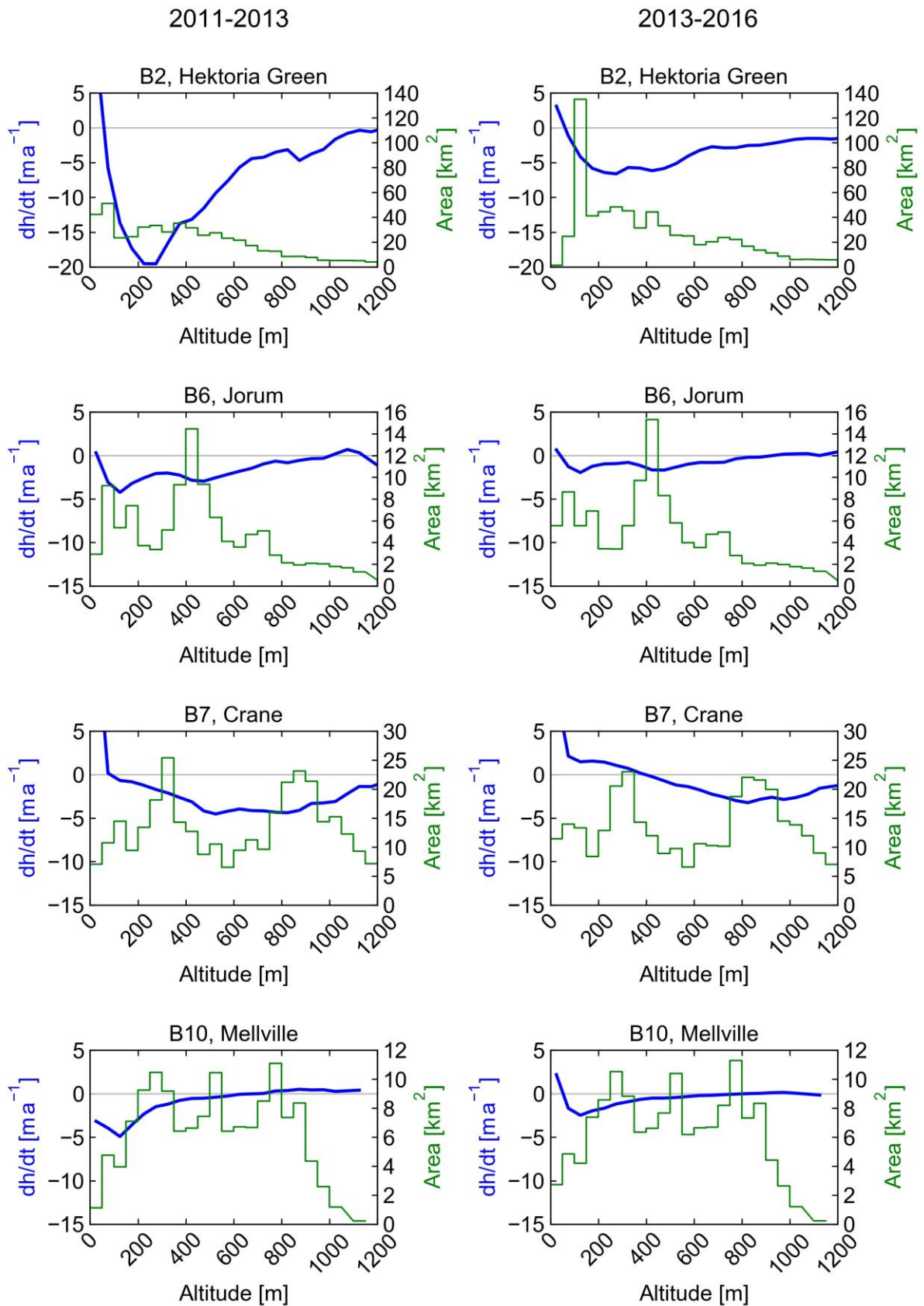


Figure 78. Rate of glacier surface elevation change dh/dt (in m a^{-1}) 2011 to 2013 and 2013 to 2016 versus altitude in 50 m intervals for basins B2. B6. B7 and B10. Green line: hypsometry of surveyed glacier area in km^2 .

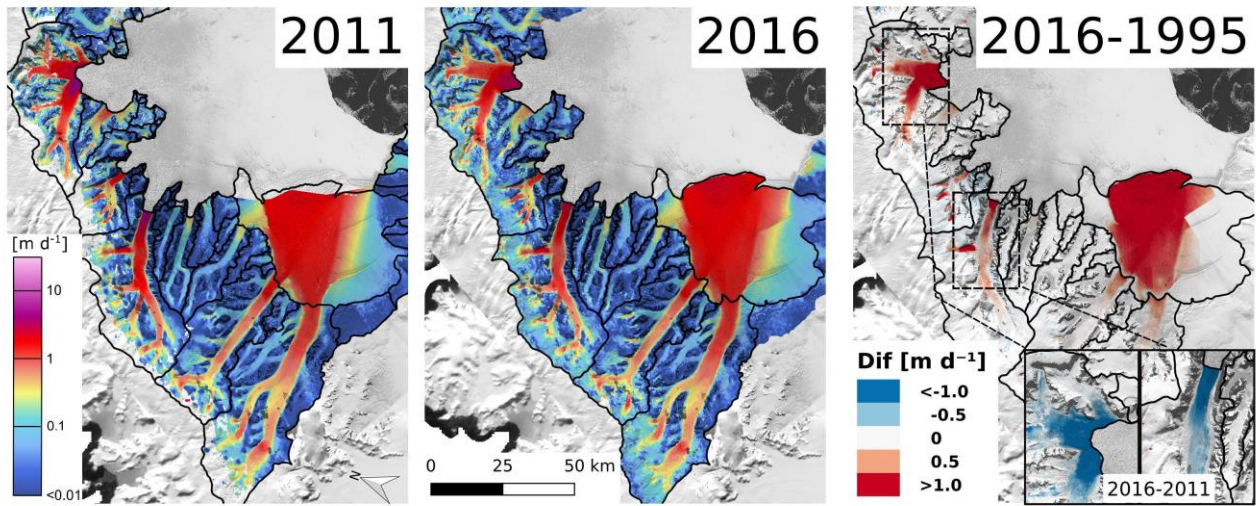


Figure 89. Magnitude of ice velocity [m d^{-1}] 2011 and 2016 derived from TerraSAR-X and TanDEM-X data. Gaps in 2011 filled with PALSAR data and in 2016 filled with Sentinel-1 data. Right: Map of velocity difference 2016 minus 1995. Insets: velocity difference 2016 minus 2011 for HG and Crane glaciers.

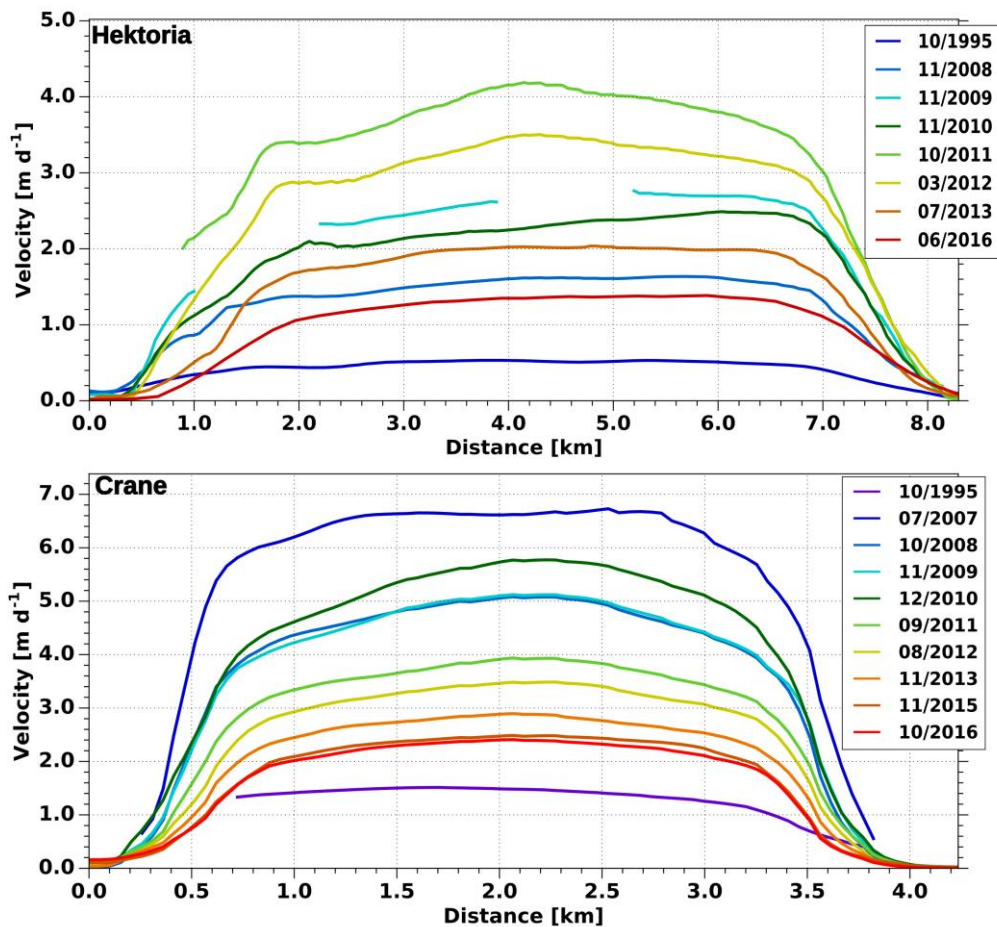


Figure 910. Surface velocity across the flux gate of Hektor Glacier and Crane Glacier on different dates (month/year) between 1995 and 2016.